



Activation kinetics of G-protein-coupled receptors

Aktivierungskinetik von G-Protein-gekoppelten Rezeptoren

Doctoral thesis for a Doctoral degree
at the Graduate School of Life Sciences
Julius-Maximilians-Universität Würzburg
Section Biomedicine

submitted by

Yevgenii Grushevskiy

from Korsun-Shevchenkivskiy, Ukraine

Würzburg 2020

Submitted on:

office stamp

Members of the Thesis Committee:

Chairperson:

Primary supervisor:

Prof. Dr. Martin J. Lohse

Supervisor (second):

Prof. Dr. Katrin G. Heinze

Supervisor (third):

Prof. Dr. Markus Sauer

Date of Public Defense:

Date of Receipt of Certificates:

AFFIDAVIT

I hereby confirm that my thesis entitled “**Activation kinetics of G-protein-coupled receptors**” is the result of my own work. I did not receive any help or support from commercial consultants. All sources and / or materials applied are listed and specified in the thesis.

Furthermore, I confirm that this thesis has not yet been submitted as part of another examination process neither in identical nor in similar form.

Place, date

Signature

EIDESSTÄTTLICHE ERKLÄRUNG

Hiermit erkläre ich an Eides statt, die Dissertation „**Aktivierungskinetik von G-Protein-gekoppelten Rezeptoren**” eigenständig, d.h. insbesondere selbständig und ohne Hilfe eines kommerziellen Promotionsberaters, angefertigt und keine anderen als die von mir angegebenen Quellen und Hilfsmittel verwendet zu haben.

Ich erkläre außerdem, dass die Dissertation weder in gleicher noch in ähnlicher Form bereits in einem anderen Prüfungsverfahren vorgelegen hat.

Ort, Datum

Unterschrift

Activation kinetics of G-protein-coupled receptors

Doctoral thesis by

Yevgenii (Eugene) Grushevskiy

ABSTRACT

G-protein-coupled receptors (GPCRs) are key biological switches that transmit both internal and external stimuli into the cell interior. Among the GPCRs, the “light receptor” rhodopsin has been shown to activate with a re-arrangement of the transmembrane helix bundle within ≈ 1 ms, while all other receptors are thought to become activated in subsecond range at saturating concentrations. Here we investigate activation kinetics of a dimeric GPCR, the metabotropic glutamate receptor-1 (mGluR1), and several class A GPCRs, as muscarinic receptor 3 (M3R), adrenergic ($\alpha 2aAR$ and $\beta 1R$) and opioid (μOR) receptors. We first used UV-light-triggered uncaging of glutamate in intact cells. Sub-millisecond Förster resonance energy transfer recordings between labels at intracellular receptor sites were used to record conformational changes in the mGluR1. At millimolar ligand concentrations the initial rearrangement between the mGluR1 subunits occurs at a speed of $\tau_1 \approx 1-2$ ms. These rapid changes were followed by significantly slower conformational changes in the transmembrane domain ($\tau_2 \approx 20$ ms). We further characterized novel photoswitchable negative allosteric modulators for mGluR1, which bind to its transmembrane core and block the conformational change as well as the downstream signaling. Effects of the compounds were quantified in pharmacological cell assays in the dark and using UV and green light illumination. We finally develop a framework for image-based kinetic analysis of GPCRs which allowed us to measure activation kinetics of several prototypical class A GPCRs and to discover membrane heterogeneities of GPCR activation. It appears that GPCR activation signal is not only dependent on the amount of activated receptors, but also has some level of correlation with the local density of activated receptors.

CONTENTS

List of figures.....	8
List of tables.....	11
Abbreviations.....	12
1. Introduction.....	15
1.1 G protein-coupled receptors.....	15
1.2 G protein-coupled receptors classification.....	17
1.3 G protein-coupled receptors activation.....	19
2. Methodology.....	25
2.1 Materials and devices.....	25
2.2 Fluorescent microscopy.....	29
2.3 Fluorescent proteins.....	30
2.4 Förster resonance energy transfer.....	32
2.5 Metabotropic glutamate receptor 1 FRET-sensors.....	35
2.6 Class A single-fluorophore sensors.....	36
2.7 Cell culture and transient transfection.....	38
2.8 Uncaging experiments.....	39

2.9	Fast epifluorescent imaging.....	42
2.10	Microplate photometry.....	43
2.11	Photoswitching.....	43
3.	Results.....	45
3.1	mGluR1 kinetics.....	45
3.2	mGluR1 photoswitchable NAM.....	52
3.3	High-throughput spatially-resolved imaging of class A GPCRs activation.....	58
4.	Discussion.....	67
5.	Summary.....	72
6.	Zusammenfassung.....	73
7.	References.....	75
8.	Curriculum Vitae.....	84
9.	Acknowledgement.....	88

List of figures

Figure 1.1. Blueprint of GPCR activity upon agonist association by a receptor.....	16
Figure 1.2. Common features of allosteric transition.....	20
Figure 1.3. Cryo-EM maps of full-length mGluR5.....	23
Figure 2.1. Jablonski diagram explaining fluorescence.....	29
Figure 2.2. Ribbon structure of GFP.....	31
Figure 2.3. Excitation and emission spectra of eCFP.....	32
Figure 2.4. Förster resonance energy transfer.....	33
Figure 2.5. FRET-based mGluR1 activation sensors.....	36
Figure 2.6. Schematic of cpGFP-based glutamate sensor.....	37
Figure 2.7. Simulated structure of D1R activation sensor with cpGFP module.....	38
Figure 2.8. Photoinduced release of glutamate from MNI-caged-glutamate.....	39
Figure 2.9. Schematic diagram of the custom built microscope setup for UV-uncaging studies..	40
Figure 2.10. Optics in the microscope setup for ligand uncaging.....	41
Figure 2.11. Schematic diagram of the microscope setup for fast imaging.....	43
Figure 2.12. Illumination of a Petri dish with SPA025-containing solution using 505 nm diode...	44
Figure 3.1. Spatio-temporal characteristics of uncaging.....	46

Figure 3.2. Activation of mGluR1 FRET sensors in living cells upon UV light-triggered uncaging of MNI-L-glutamate.....	48
Figure 3.3. Millisecond kinetics of the E-sensor and the A-sensor activation.....	49
Figure 3.4. Dependence of mGluR1 E-sensor activation on UV-pulse duration and laser power...	50
Figure 3.5. Effects of the C254E mutation on FRET-signals of the mGluR1 E- and A-sensors.....	51
Figure 3.6. mGluR1 NAM.....	53
Figure 3.7. Photoisomerization of SPA025.....	54
Figure 3.8. Wide-field images of HEK293T cells expressing mGluR1 intramolecular FRET-sensor on a bottom of microtiter plate.....	55
Figure 3.9. Quantification of SPA025 affinity to mGluR1 in presence of 100 μ M L-glutamate....	56
Figure 3.10. SPA025-dependent activation of mGluR1 upon L-glutamate stimulation.....	57
Figure 3.11. Concentration responses of SPA025-1 isomers on intracellular IP1 production measured using the HTRF-IP1 assay.....	58
Figure 3.12. Activation of M3R-cpGFP.....	59
Figure 3.13. Workflow of single-pixel analysis of α 2aAR-cpGFP.....	61
Figure 3.14. Schematics of the applied fit to each individual pixel during the kinetic analysis.....	62
Figure 3.15. α 2aAR kinetic analysis of distinct pixels.....	63
Figure 3.16. mGluR1 activation kinetics measured with single-pixel analysis.....	63
Figure 3.17 μ OR activation kinetics.....	64

Figure 3.18. β 1AR activation kinetics.....65

Figure 3.19. Whole cell GPCR activation deviates from receptor-concentration dependency.....66

Figure 3.20. Schematic illustration of the activation and deactivation kinetics in mGluR1s.....69

List of tables

Table 1. Chemical and reagents used in cell culture and transient transfection.....	25
Table 2. Ligands and other chemicals.....	26
Table 3. Optical elements used in microscope setup for uncaging.....	26
Table 4. Devices in uncaging setup.....	27
Table 5. Devices and kits used for high-throughput experiments with photo-NAM.....	27
Table 6. Optical elements used in imaging setup.....	28
Table 7. Devices in the setup for fast imaging.....	28
Table 8. List of used plasmids.....	28

ABBREVIATIONS

α 2aAR: α 2a-adrenergic receptor

β 1AR: β 1-adrenergic receptor

β 2AR: β 2-adrenergic receptor

AC: Adenylyl cyclase

AP2: adaptor protein 2

BRET: Bioluminescence resonance energy transfer

BSA: Bovine serum albumin

cAMP: Cyclic adenosine monophosphate

CaSR: Calcium-sensing receptor

CFP: Cyan fluorescent protein

cpGFP: Circularly permuted green fluorescent protein

CRD: Cysteine rich domain

CMNB-fluorescein: (5-Carboxyfluorescein-Bis-(5-Carboxymethoxy-2-Nitrobenzyl) Ether,

β -Alanine-Carboxamide

DMEM: Dulbecco's modified Eagle's medium

EC50: Half maximal effective concentration

ECD: extracellular domain

EGFP: Enhanced green fluorescent protein

EM: Electron microscopy

ERK: Extracellular-signal regulated kinase1/2

FDA: Food and Drug Administration (US health agency)

FP: Fluorescent protein

FRET: Fluorescence resonance energy transfer

GABAB: γ -aminobutyric acid receptor B

GDP: Guanosine diphosphate

GFP: Green fluorescent protein

GIRK: G-protein-coupled inwardly rectifying potassium channel

GPCR: G-protein-coupled receptor

GRK: G-protein-coupled receptor kinase

HBSS: Hank's balanced salt solution

HEK: Human embryonic kidney

HTRF: Homogeneous time resolved fluorescence

IC50: Half maximal inhibitory concentration

IP1: Inositol-1,4,5-trisphosphat

M3R: muscarinic receptor 3

MCR2: Melanocortin receptor 2

MD: Molecular dynamics

MNI-glutamate: 4-methoxy-7-nitroindolinyl-glutamate

MOR: μ -opioid receptor

MTR Melatonin receptor

NAM: Negative allosteric modulator

NMR: Nuclear magnetic resonance

PAM: Positive allosteric modulator

PDB: Protein Data Bank

PIP2: Phosphatidylinositol-4,5-bisphosphate

PLC β : Phospholipase C

PKA: Protein kinase A

PKC: Protein kinase C

sCMOS: Scientific complementary metal–oxide–semiconductor

TM: Transmembrane domain

TTL: Transistor-transistor logic

VFT: Venus flytrap

YFP: Yellow fluorescent protein

1. INTRODUCTION

1.1. G-protein-coupled receptors

G-protein-coupled receptors (GPCRs) mediate most of the cellular responses to external stimuli such as light, ions, hormones, neurotransmitters, peptides, metabolites and odors¹. GPCRs are membrane proteins consisting of seven transmembrane (TM) α -helices. The ligands that activate them stabilize the conformation of receptor that can interact with the heterotrimeric G-protein, facilitating the exchange of GTP for GDP from the $G\alpha$ subunit. GTP-bound $G\alpha$ dissociates from $G\beta\gamma$, and $G\alpha$ and $G\beta\gamma$ independently trigger signaling intracellular cascades². In addition to signaling via G-proteins, GPCRs can also transmit signals through arrestins³ (Figure 1.1). Arrestins were first described as proteins that terminate the G-protein signal: phosphorylation of the C-terminal tail of the receptor using the G-protein-coupled receptor kinase (GRK) leads to the recruitment of arrestin, which precludes interaction with G-proteins and promotes the internalization of receptors. However, some GPCR ligands can induce arrestin binding directly or, possibly, by stimulating interaction with GRKs to allow arrestin binding, thereby activating downstream signaling pathways other than those mediated by G-proteins⁴.

A small portion of well-studied GPCRs already account for about 34% of all medications approved by US Food and Drug Administration (FDA), emphasizing their essential role in health and disease⁵. Scientific knowledge has evolved rapidly over the last fifteen years due to breakthroughs made through the application of structural and biochemical GPCR studies, especially advances in protein purification and engineering, lipid crystallography, X-ray diffraction, and cryo-EM⁶.

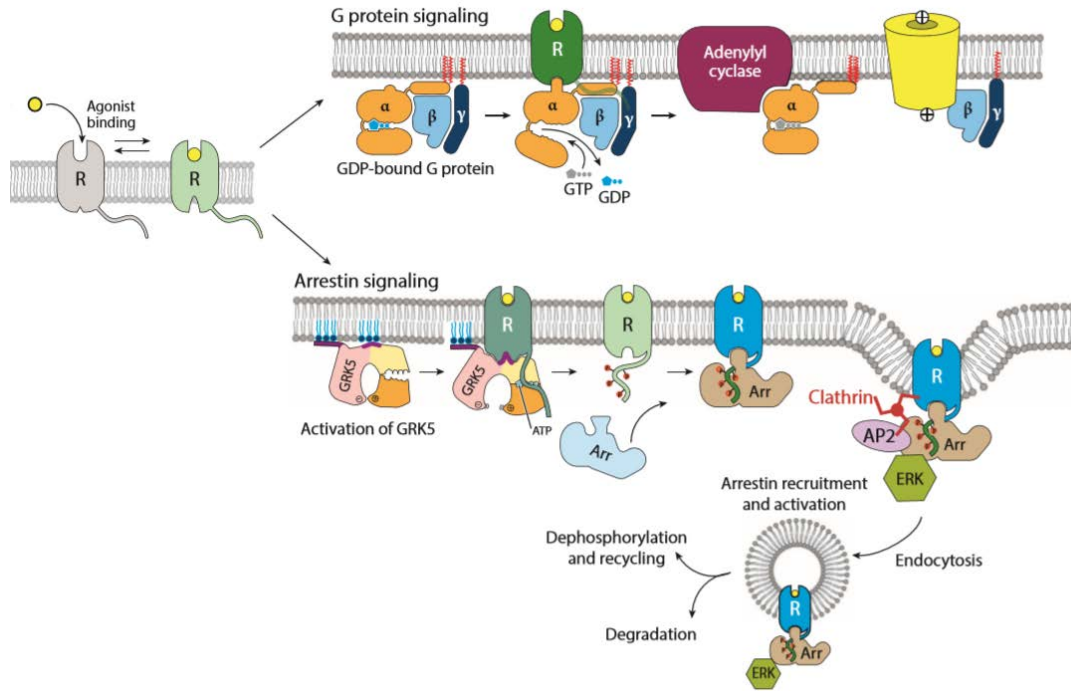


Figure 1.1. Blueprint of GPCR activity upon agonist association by a receptor. Classical G-protein pathway. Top, exchange of GDP for GTP in the G protein α subunit leads to dissociation and interaction with downstream effectors such as $G_{\alpha s}$ stimulation of adenylyl cyclase (AC) and $G\beta\gamma$ activation of ion channels. Bottom, activated GPCRs can also signal *via* arrestins. Phosphorylation of the receptor C-terminal tail by a G-protein–coupled receptor kinase promotes arrestin (Arr) recruitment and activation, including endocytosis through interactions with the clathrin adaptor protein 2 (AP2) complex and activation of extracellular signal-regulated kinase (ERK)⁷. (adapted from Weis and Kobilka, *Annu Rev Biochem*, 2018)

As of today, there are more than 200 reported GPCR structures (PDB entries) from more than 50 unique receptors. These structural studies have provided new insights into the nature of GPCR activation, modulation by exogenous and endogenous molecules, and dimerization⁶.

1.2. G-protein-coupled receptors classification

More than 800 GPCRs are encoded in the human genome, which makes them the largest superfamily of cell-surface receptors and takes up about 4% of the entire protein encoding genome⁸.

As per classical A-F system, GPCRs can be sorted into 6 classes based on sequence homology and functional similarity:

Class A	Rhodopsin-like
Class B	Secretin receptor family
Class C	Metabotropic glutamate/pheromone
Class D	Fungal mating pheromone receptors
Class E	Cyclic AMP receptors
Class F	Frizzled/Smoothed

In other studies, an alternative classification system called GRAFS (**G**lutamate, **R**hodopsin, **A**dhesion, **F**rizzled/Taste2, **S**ecretin) has been proposed based on phylogenetic analysis of vertebrate GPCRs. To avoid confusion, only A-F classification will be used below. In this study we are focused only on kinetic investigations of class A and C receptors.

Class A. About 85% of GPCRs belong to the so-called class A or rhodopsin-like receptors, which are the most well-studied group. Class A includes the receptors for light (rhodopsin), adrenaline (adrenergic receptors), chemokines, opioids, neuropeptides, cannabinoids and many other 7-TM receptor types, including olfactory subgroup. Despite the fact that their activating ligands vary widely in structure and kind, the amino acid sequences of the class A receptors are very similar and are believed to adopt a common structural framework comprising 7-TM helices⁹. Structural and

spectroscopic data suggest that conserved structural elements result in very similar functional conformations. Differences of sequences adjust the relative energies of these conformations and the barriers between them. Recent structural evidence suggests that many of the general principles disclosed in family A receptors apply to other GPCR families.

Class C. Crystallographic data and comparative observations suggest that class C GPCRs evolved from a common ancestor that belonged to the bacterial nutrient periplasmic binding protein family¹⁰. These proteins share a bilobed structure reminiscent of a Venus flytrap (VFT): a structure containing two protomers that are separated by a cleft region. Class C includes metabotropic glutamate receptors (mGluRs), calcium-sensing receptor (CaSR), basic amino acid receptors, for example GPRC6A, sweet and umami taste receptors (e.g., T1R1 and -3), pheromone receptors (e.g. V2R in vomeronasal organ), and γ -amino-butyric acid (i.e., GABA_BR1 and -2). Although members of class C are molecularly different, their pharmacological profiles overlap. For instance, Ca²⁺ is the physiological ligand at the CaSR, but several amino acids allosterically modulate receptor sensitivity for this ion. Similarly, amino acids, GABA, and certain nutrients act as orthosteric agonists at mGluRs, GPRC6A, GABA_BRs, and T1Rs, and Ca²⁺ can modulate these responses. Class C GPCRs function as obligate dimers (either homo- or heterodimers). Homodimerization has been demonstrated for mGluRs¹¹, CaSR¹², and GPRC6A¹³, whereas GABA_B¹⁴ and T1Rs¹⁵ are constitutive heterodimers. In addition, CaSR, mGluRs, and GABA_B can also heterodimerize, giving rise to novel functional units with pharmacological profiles and plasma membrane expression different from that of their native homodimeric assemblies. Specifically, CaSR heterodimers include (a) CaSR/mGluR1a and CaSR/mGluR5 and (b) CaSR/GABA_BR1 and CaSR/GABA_BR2. Crystallographic data obtained from the extracellular domain of mGluR show that the two lobes of the VFT exist in open and closed conformations. Agonist binding occurs in the

pocket of lobeI, which subsequently promotes the closure of lobeII, a process that brings about the conformational change necessary for signal transmission¹⁶.

1.3. G-protein-coupled receptors activation

GPCRs are allosteric by definition, since they translate environmental signals between spatially different but conformationally linked parts of the protein. In response to the association of agonists with the orthosteric site, GPCR transforms through conformational changes that makes it capable to interact with internal transducers, such as heterotrimeric G-proteins and arrestins, which eventually results in an integrated cellular cascade.

Intuitively, the most straightforward mechanism of GPCR activation is a conformational selection mechanism consisting of two states with a so called “allosteric transition” mediating a change between inactive and active states. Agonists predominantly stabilize the active state, inverse agonists stabilize the inactive state, while neutral antagonists show a similar relationship to both states, but can block the actions of both agonists and inverse agonists if they interact through a site that overlaps. Many GPCRs can signal in the absence of endogenous agonists, a phenomenon called basal activity.

Rhodopsin is a prototypical receptor that illustrates this mechanism, and numerous structures have been reported that follow key states of rhodopsin (Figure 1.2). However, rhodopsin function as a light sensor is uniquely distinctive for sensitivity and fidelity. In the inactive state, rhodopsin is covalently bound to its ligand, 11-*cis*-retinal, which acts as a highly effective inverse agonist to suppress basal activity. Such virtual absence of basal activity ensures high signal fidelity in the visual system.

Illumination by light isomerizes the 11-*cis*-retinal into all-*trans*-retinal agonist, leading to an allosteric transition, which is completed by the 6-8 Å displacement of transmembrane helix 6 (TM6) from the transmembrane bundle, thereby creating an intracellular binding site. Other common structural changes that accompany GPCR activation include receptor top contraction, TM5 and TM7 inward movement, and TM3 rotation¹⁷.

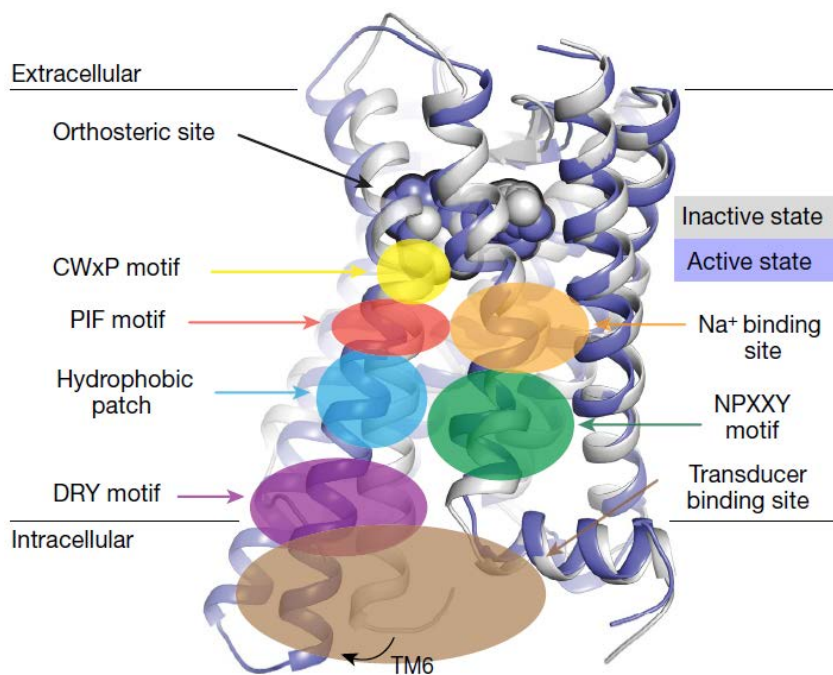


Figure 1.2. Common features of allosteric transition. Different motifs, sodium- and transducer-binding sites mapped onto inactive and active states of rhodopsin, PDB: 1F88 and PDB: 3PQR respectively¹⁸ (adapted from Thal *et al.*, Nature, 2018)

These changes are supposedly facilitated by the restructuring of the conserved allosteric network of neighboring residues, or microswitches, and water molecules¹⁹, common to most GPCR class A sites, and they are key components of the allosteric link between the orthosteric and intracellular transducer sites, which are typically located at a distance of ~ 40 Å or more.

Nevertheless, there is a constantly growing amount of evidence provided by NMR spectroscopy and molecular dynamics simulations that functional diversity of GPCRs is due to structural plasticity. GPCRs can no longer be described as simple bimodal switches, but rather exist as ensembles of multiple discrete conformations with energy profiles that can be affected by ligands, cytosolic signaling and regulatory proteins, lipids, pH, ions and possibly transmembrane voltage gradients²⁰.

So far, the activation kinetics have been elucidated in detail only for one GPCR, the light receptor rhodopsin²¹. This is because rhodopsin can be activated synchronously by light; upon activation the covalently bound retinal undergoes spectral changes that allow precise recording with optical methods; and in rod outer segments rhodopsin represents $\approx 95\%$ of protein, allowing easy experimental access. Following light activation rhodopsin adopts its active meta-II state, characterized by a re-arrangement of the TM helix bundle, within about one millisecond via a series of short-lived intermediate receptor conformations^{22,23}.

For all other GPCRs, activation is thought to be much slower^{23,24}. Functional studies measuring receptor-triggered ion currents gave activation time constants of a few seconds for the entire signaling chain, which could be reduced down to ≈ 200 ms upon strong receptor overexpression²⁵. Initial studies with purified, fluorescently labelled and reconstituted receptors reported conformational changes over many seconds^{26,27}. Later biophysical studies on non-rhodopsin GPCRs with single molecule fluorescence, NMR and molecular dynamics simulations identified rapid dynamic transitions within and between different off- and on-states in the sub-ms to hundreds of ms time range²⁸⁻³³. Additionally, these studies indicated that the fully active state of non-rhodopsin GPCRs requires stabilization by binding to a G-protein or to a β -arrestin^{32,33}. However, none of these studies provided rapid agonist-induced activation kinetics. In intact cells,

agonist-induced activation of non-rhodopsin GPCRs has been studied by using FRET-based sensors combined with rapid changes in superfusion media. For most GPCRs, these studies have yielded agonist-induced activation time constants in the 30-80 ms range³⁴⁻³⁶.

As the first target for kinetic investigations we chose mGluR1³⁷, a prototypical class C GPCR, because of its interesting activation mode and because earlier studies with this receptor yielded relatively fast activation time constants³⁸⁻⁴⁰. mGluR1 are activated by the excitatory neurotransmitter L-glutamate and, as other class C members, possess large N-terminal extracellular domains (ECDs) that form mandatory dimers and contain the orthosteric ligand-binding sites. ECD in turn is composed of a conserved bilobed ligand-binding VFT domain and a cysteine-rich domain (CRD). The VFT is connected to the 7-TM domain by the CRD, which provides a semi-rigid linker between the ligand-binding and the 7TM domains³⁷.

Initial structural studies with VFT in isolation have shown that agonist binding triggers two major structural changes in the dimer conformation. The first is the closure of the two VFT lobes. Live cells studies have shown that closing of one VFT is enough to transmit the signal, while closure of both VFTs is necessary to achieve full activation¹⁶. The second conformational step implicates intersubunit reorientation, which brings the CRDs of neighboring VFTs in close proximity to each other (Figure 1.3). Previous studies in our lab using fluorescence resonance energy transfer of full-sized receptors in live cells have shown that activation depends on consecutive inter- and intrasubunit conformational changes³⁹.

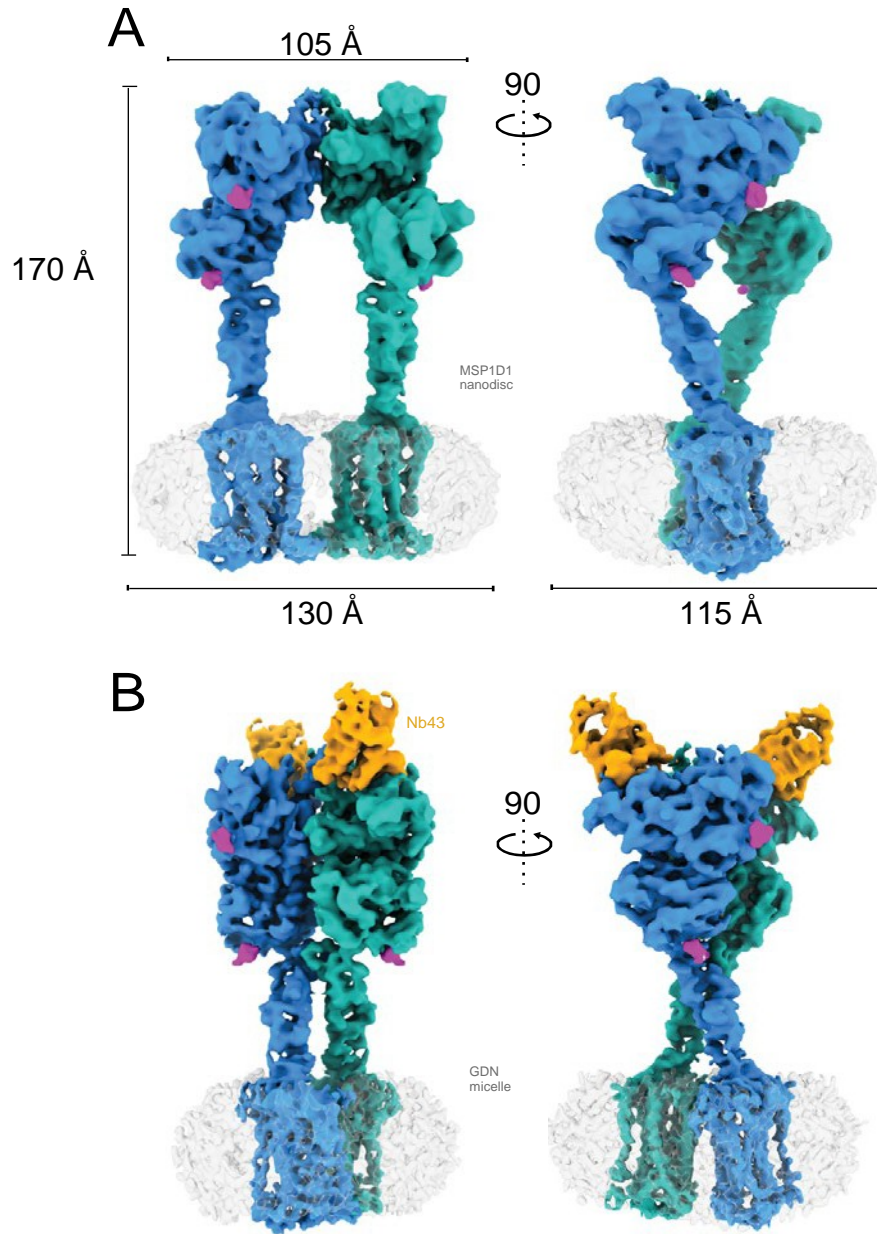


Figure 1.3. Cryo-EM maps of full-length mGluR5. Apo-VFT state (A) and the active state bound to Nb43 and quisqualate (B)⁴¹. (adapted from Koehl *et al*, Nature, 2019)

A type of molecules that bind to spatially distinctive allosteric sites to modulate the effects of orthosteric ligands is called allosteric modulators. Positive allosteric modulators (PAMs) enhance activity of orthosteric ligands and negative allosteric modulators (NAMs) hinder activity. Neutral

allosteric ligands (NALs) have no effect on the activity, but competitively block the effects of PAMs or NAMs that bind to the same allosteric site⁴². So-called 'bitopic' molecules, which bridge both orthosteric and allosteric sites on a single GPCR, have also been investigated in recent years.

2. METHODOLOGY

2.1. Materials and devices

Item	Manufacturer	Miscellaneous
DMEM	PAN Biotech	P04-03600
Fetal calf serum	Biochrom AG	
Penicillin-streptomycin	Gibco	15140122
L-glutamine	PAN Biotech	P04-80050
BSA	AppliChem	A1391
Sodium pyruvate	Sigma-Aldrich	P8574
Glutamate-pyruvate transaminase	Roche	
DMEM-GlutaMAX	Gibco	10566016
HBSS 10x	Gibco	14185-045
Poly-D-lysine	Sigma-Aldrich	A-003
Effectene Transfection Reagent	Qiagen	

Table 1. Chemical and reagents used in cell culture and transient transfection

Item	Manufacturer	Miscellaneous
MNI-caged-glutamate	Tocris	1490
CMNB-fluorescein	ThermoFisher Scientific	C20050
Norepinephrine	Sigma-Aldrich	
Morphine	Sigma-Aldrich	
DAMGO	Sigma-Aldrich	

Table 2. Ligands and other chemicals

Item	Manufacturer	Miscellaneous
DCLP 420-45	unknown	purchased from Rapp Optoelectronics
HC BS 442	Semrock	purchased from AHF, F38-442
HC BS 509 imaging	Semrock	purchased from AHF, F38-508
405 LP laser BrightLine single-edge	Semrock	
483/32 BrightLine HC	Semrock	purchased from AHF, F37-483
ET BP 535/30	Chroma	purchased from AHF, F47-535
Quartz coverslips \varnothing 25 mm	Ted Pella, Inc.	
Fluar 100x/1.30 Oil UV	Zeiss GmbH	purchased from Rapp Optoelectronic
Camera adapter 60N-C 0.5x	Zeiss GmbH	purchased from Rapp Optoelectronic
Axio Observer D1	Zeiss GmbH	purchased from Rapp Optoelectronic

Table 3. Optical elements used in microscope setup for uncaging

Item	Manufacturer	Miscellaneous
pe-4000 LED system	CoolLED	with TTL expansion box EB25D
UV laser	Rapp Optoelectronics	DL 375
sCMOS camera	Thorlabs	DCC3240N
Analog-to-digital converter	Molecular Devices	Axon Digidata 1550
Photomultiplier	ET Enterprises Ltd.	9085B Series
Photometer amplifier	Myotronic	
Iris Diaphragm Tube	Linos	Mounting system C

Table 4. Devices in uncaging setup

Item	Manufacturer	Miscellaneous
Multi-Mode Reader	BioTek Instruments	Synergy Neo2
Cell counter	Thermo Fisher Scientific	Countess II FL
Microtiter plates	Brand GmbH+Co KG	96-well F-bottom plates
HTRF-IP1 kit	Cisbio	Tb2+-cryptate
Collimator	Thorlabs GmbH	COP-1A
LED system	CoolLED	pe-4000

Table 5. Devices and kits used for high-throughput experiments with photo-NAM

Item	Manufacturer	Miscellaneous
T505lpxr	Chroma	
ET 470/24 M	Chroma	310325
ET535/30 M	Chroma	308583
520/35 BrightLine HC	Semrock	
Dual-band excitation filter	Chroma	59017X, 314226
Dual-band emission filter	Chroma	59017M, 314976
HC PL APO 63×/1.40-0.60 oil	Leica Microsystems	
D/F/Cy3/Cy5 sbxm ET filter set	Chroma	purchased from AHF F55-890
DMi8	Leica Microsystems	

Table 6. Optical elements used in imaging setup

Item	Manufacturer	Miscellaneous
Polychromator	Visitron Systems GmbH	VisiChrome
sCMOS camera	Teledyne Photometrics	Prime 95B
Image-splitter	Cairn Research	OptoSplit II
Perfusion system	ALA Scientific Instruments	ALA-VM8
Digital valve control system	ALA Scientific Instruments	Octaflow II

Table 7. Devices in the setup for fast imaging

Plasmid	Vector	Source
mGluR1 E-sensor	pcDNA3	Institute of Pharmacology, Würzburg
mGluR1 A-sensor	pcDNA3	Institute of Pharmacology, Würzburg
mGluR1 E-sensor-(C254E)	pcDNA3	Institute of Pharmacology, Würzburg
mGluR1 A-sensor-(C254E)	pcDNA3	Institute of Pharmacology, Würzburg
M3R-cpGFP	pDisplay	addgene
α 2aA-cpGFP	pTwist-CMV	Synthesized by Ali Isbilir in the lab
μ OR-cpGFP	pTwist-CMV	Synthesized by Ali Isbilir in the lab
β 1AR-cpGFP	pTwist-CMV	Synthesized by Ali Isbilir in the lab

Table 8. List of used plasmids

2.2. Fluorescent microscopy

Electrons in molecules during the absorption of light, mechanical or chemical action can go into an excited state. When electrons transition from an excited state to a ground state, or from an excited state with a higher energy to an excited state with a lower energy, some sensitive molecules can emit. This phenomenon is called luminescence. The phenomenon of radiation by a molecule or atom of light when a photon excites ultraviolet light or visible light is called photoluminescence, which, depending on the electronic configuration of the excited state and the radiation process, is formally divided into fluorescence and phosphorescence. Fluorescence is the property of certain atoms or molecules to absorb light of a particular wavelength and emit light with a longer wavelength over a short time interval, called the duration of fluorescence.

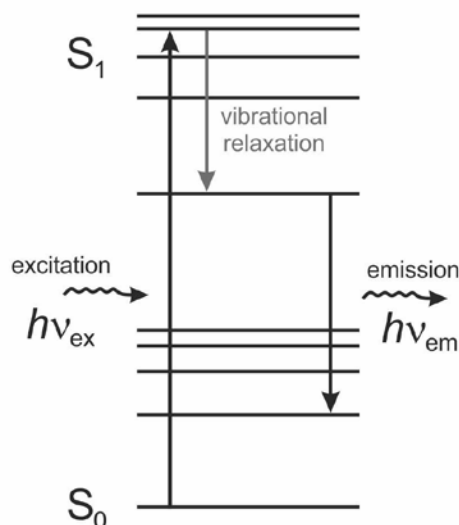


Figure 2.1. Jablonski diagram explaining fluorescence. A molecule absorbs a high-energy photon which excites the system electronically and vibrationally. Eventually, the system relaxes and a lower-energy photon emission can occur.

Today, fluorescence microscopy is widely used in medical and biological research. This is due to the fact that this type of microscopy opens up new possibilities for research, unattainable when using simple microscopes. Therefore, the widespread use of fluorescence microscopy has led to the emergence of more sophisticated microscopes and instruments that allow the use of fluorescence research methods.

Fluorescence microscopy, unlike other types of light microscopy, allows to display the distribution of individual molecules only by using the properties of fluorescence radiation. Thanks to fluorescence microscopy, it became possible to track the location of individual components of the cell, as well as their diffusion coefficients, transport characteristics and interaction with biomolecules. A significant dependence of fluorescence on changes in external factors allows us to study pH, viscosity, refractive index, solution polarity, ionic concentrations and membrane potentials in living cells and cell cultures.

2.3. Fluorescent proteins

Progress in cell biology imaging is associated with the discovery, genetic cloning, and heterologous expression of jellyfish *Aequorea victoria* green fluorescent protein (avGFP). Expression of the protein itself or many of its genetic associations with other proteins leads to visible fluorescence when the sample is irradiated with near ultraviolet light⁴³. Green fluorescent protein (Figure 2.2) is just one member of a family of homologous fluorescent proteins. They stand out mainly from seahorses and jellyfish, and have different colors, which are determined by the variety of chromophore covalent structure and non-covalent environment.

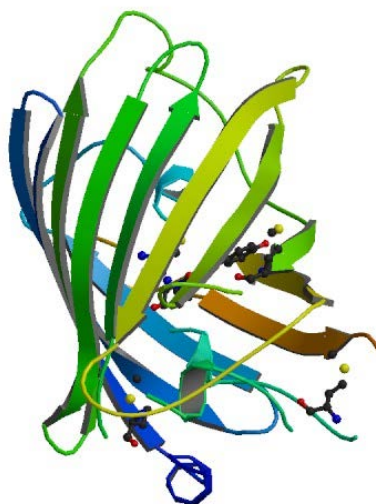


Figure 2.2. Ribbon structure of GFP (adapted from PDB <https://www.rcsb.org/structure/1EMA>)

Laboratory mutagenesis further diversified the spectrum of fluorescent proteins, increased their brightness and stacking efficiency, and also reduced oligomerization⁴⁴. A mutation can both increase photostability for standard observation of fluorescence^{45,46}, and generate fluorescent proteins that will act as “photorelay” from dark to bright and from one color to another^{47,48}. The “photorelay effect” can be reversed and irreversible and can be useful for tracking protein diffusion, protein traffic and age. It has already become possible to induce a mutation of the fluorescent protein, so that it causes photodestruction of cells⁴⁹. In general, fluorescence of fluorescent proteins is quite high compared to the environment in which they are located; quenching of fluorescence occurs only in an acidic environment ($\text{pH} < 7$) and during denaturation, but there are also fluorescent proteins designed for increased sensitivity to pH ⁵⁰⁻⁵² and susceptibility to metals^{53,54}, halogen ions⁵⁵ or reductive oxidative potentials⁵⁶⁻⁵⁹. In this work, we used GFP color mutants, enhanced cyan fluorescent protein (eCFP), spectra of which are shown in

Figure 2.3, enhanced yellow fluorescent protein (eYFP), and circularly permuted green fluorescent protein (cpGFP).

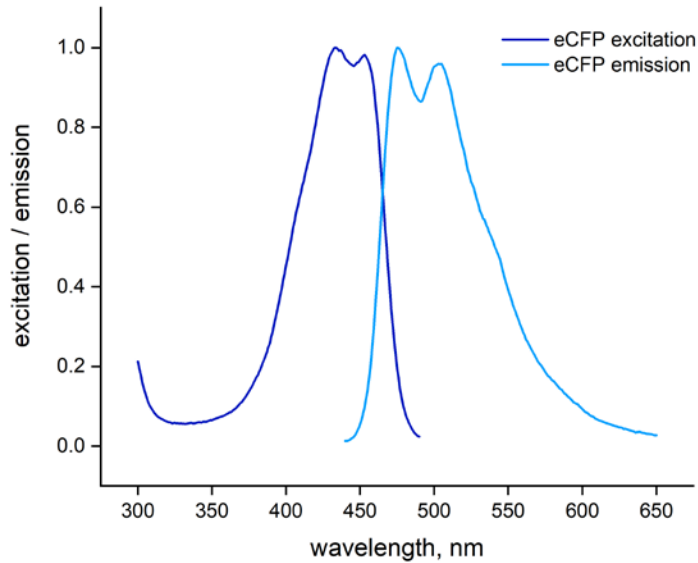


Figure 2.3. Excitation and emission spectra of eCFP.

2.4. Förster resonance energy transfer

Förster resonance energy transfer (FRET) is a nonradiative mechanism of energy transfer from a donor fluorophore to an acceptor fluorophore typically over distances of about 10-90 Å. The dependency between fluorophore distance and energy transfer was initially described by Förster in 1948⁶⁰ and was later confirmed by Stryer and colleagues, in the 1970's⁶¹. Sensitivity of fluorescence-based detection, fast energy transfer, and convenient distance of interaction of fluorophores are among the advantages of FRET.

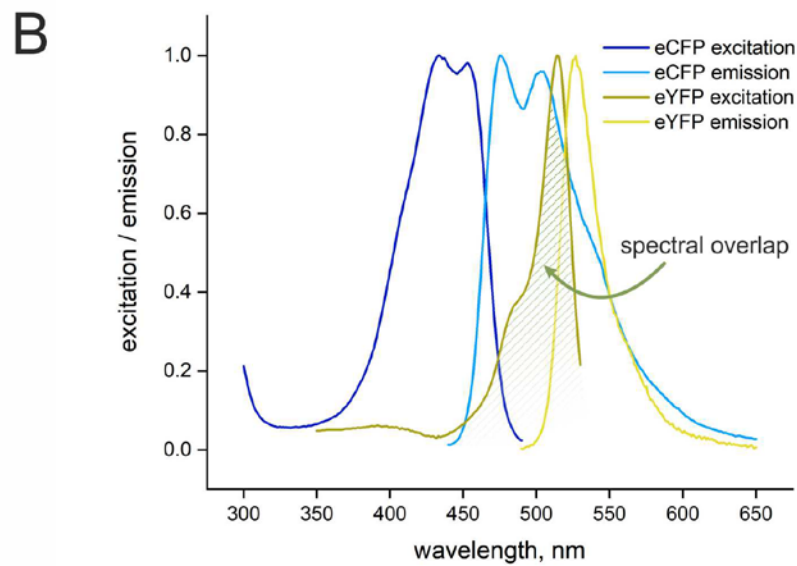
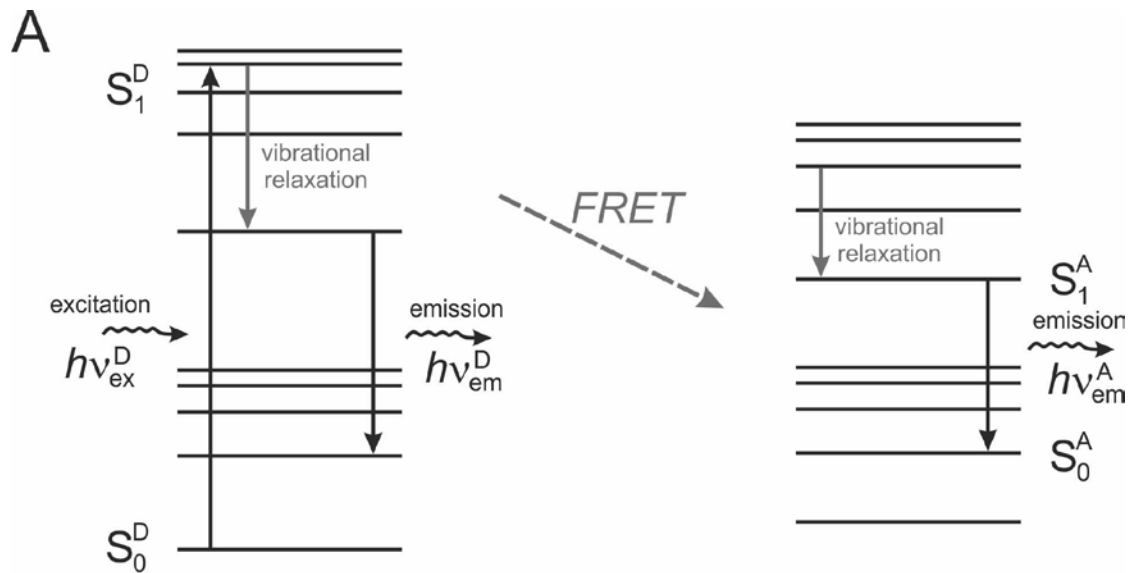


Figure 2.4. Förster resonance energy transfer. (A) Jablonski diagram explaining FRET. Donor molecule absorbs a photon which excites the molecule electronically and vibrationally. In the near-field region, the excited chromophore emits a so-called “virtual photon” that is instantly absorbed by an acceptor chromophore. (B) Excitation and emission spectra of eCFP and eYFP with the marked spectral overlap, which is one of the mandatory requirements for FRET.

Molecular processes causing FRET have been studied extensively and are illustrated in Figure 2.4A. The first step encompasses absorption of energy (photons) by the donor molecule, resulting in excitation from the ground singlet state, S_0^D , to an excited singlet state, S_1^D . Several excited states are available to the donor; however, vibrational relaxation to S_1^D by internal conversion is fast, ensuring that most of emission occurs from this state. Several outcomes are available for the excited donor, including spontaneous emission and nonradiative processes. If a suitable acceptor fluorophore is nearby, then nonradiative energy transfer between the donor and acceptor can occur. This transfer involves a resonance between the singlet-singlet electronic transitions of the two fluorophores, generated by coupling of the emission transition dipole moment of the donor and the absorption transition dipole moment of the acceptor. Thus, the efficiency of FRET and the range of distances over which it can be observed are determined by the spectral properties of a given donor acceptor pair. In other words, parameters for successful FRET can be grouped as:

- 1) the distance between the donor and the acceptor molecules is in the range of 1–10 nm;
- 2) acceptor absorption spectrum overlaps with the donor emission spectrum (Figure 2.4B);
- 3) suitable relative orientation of the donor emission dipole moment and the acceptor absorption dipole moment.

Since many years the most common pair of fluorophores for biological use is a cyan fluorescent protein (CFP) and yellow fluorescent protein (YFP)⁶². Both are color variants of green fluorescent protein (GFP). To avoid having external illumination, which might lead to high background signal,

bioluminescence resonance energy transfer (BRET) has been developed⁶³. This technique uses same physical principle but a bioluminescent luciferase (usually the luciferase from *Renilla reniformis*) rather than CFP to produce an initial photon emission compatible with YFP.

2.5. Metabotropic glutamate receptor 1 FRET-sensors

To study the kinetics of intermolecular activation of mGluR1 receptors, a family of sensors was previously created by attaching CFP or YFP to one of two sites in the receptor: either built into the intracellular loop 2 between Ile685 and Leu686, or added at the C-terminus (*E*-sensor, Figure 2.5A). To study the kinetics of intramolecular activation, sensors containing both YFP and CFP were created, one at each site (*A*-sensor, Figure 2.5B). To control 1:1 stoichiometry of the subunit composition of mGluR1 dimers, the C-terminal “quality control system” of the GABA_B receptor was used. In these sensor families, the C-terminus of mGluR1 subunits was replaced by either the last 87 C-terminal amino acids of GABA_{B1} (c1), the first 62 amino acids of the C-terminal tail of GABA_{B1} (c1sh), or the last 181 C-terminal amino acids of GABA_{B2} (c2), or the first 61 amino acids of the C-terminal tail of GABA_{B2} (c2sh). so that only heterodimers containing two different longer C-terminal tails (version c1 and version c2) reach the cell surface³⁹. An *A*-sensor having short C-terminal tails has reached the cell surface.

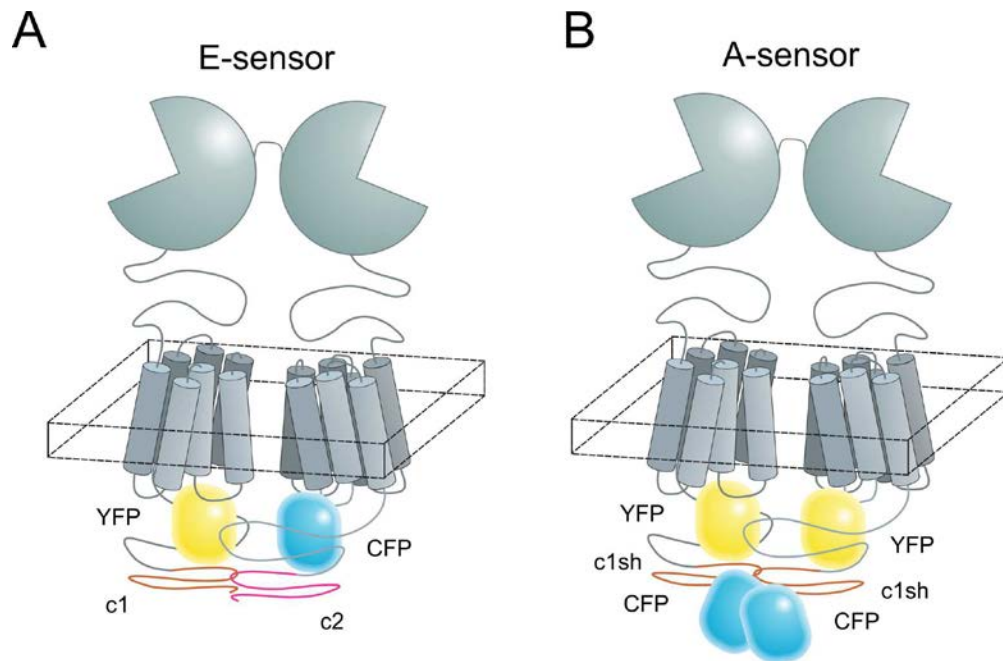


Figure 2.5. FRET-based mGluR1 activation sensors. Schematic of the *E*- (A) and *A*-sensors (B), reporting *intermolecular* and *intramolecular* movements of the mGluR1, respectively.

The *E*-sensor is composed of one mGluR1 labelled with a CFP, and one labelled with a YFP in the 2nd intracellular loop; a C-terminal tail from the GABA_{B1} and GABA_{B2} receptor, respectively, assures that only dimers carrying two different labels reach the cell surface ³⁹. The *A*-sensor contains two mGluR1 protomers, each labelled with a YFP in the 2nd intracellular loop and a CFP at the C-terminus.

2.6. Class A single-fluorophore sensors

Besides FRET-based receptor activation sensors we also made use of recently developed single-fluorophore activation sensors to study class A GPCRs. Single-wavelength indicators are

typically based on circularly permuted or split fluorescent proteins and showed to be an attractive alternative. In the beginning, reporters for calcium⁶⁴ and glutamate⁶⁵ (Figure 2.6) were described using cpGFP.

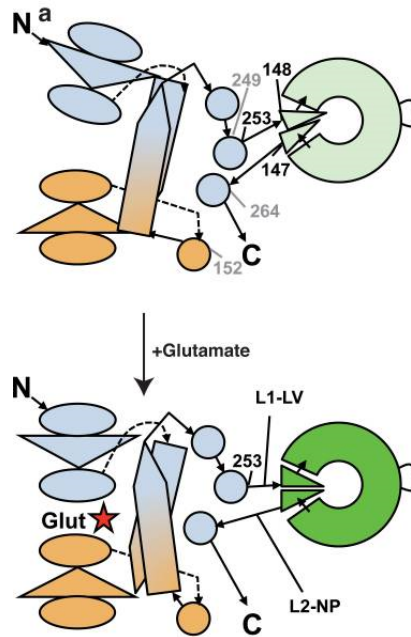


Figure 2.6. Schematic of cpGFP-based glutamate sensor. Blue and orange represent the binding site for glutamate. The polypeptide chain starts in the N-terminal domain (blue), passes into the C-terminal domain (orange) and continues back through two β -strands (long pointed shapes) and into a series of helices (circles). The open (top), ligand-free state of the construct is dim, because of distortion of the cpGFP β -barrel (tilted triangles). Binding of glutamate (star) induces a conformational change. The closed (bottom) state is bright, due to restoration of the β -barrel⁶⁵.

(adapted from Marvin *et al.*, Nature Methods, 2013)

Later on, such sensors were introduced in muscarinic (M1-5R)⁶⁶, dopamine (D1R), adrenergic (α 2, β 1,2AR), opioid (κ , μ OR), serotonin (5HT2AR) and melatonin (MTR) receptors⁶⁷.

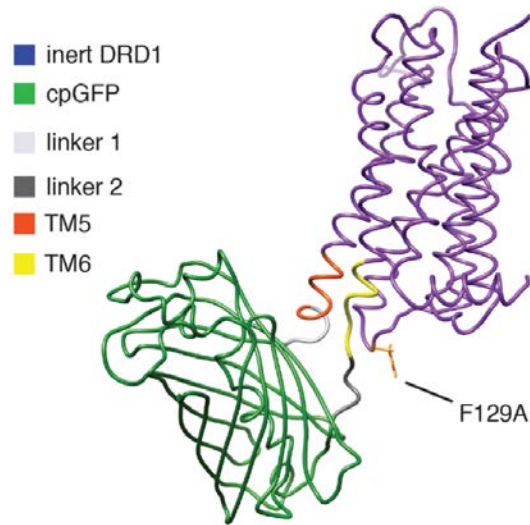


Figure 2.7. Simulated structure of D1R activation sensor with cpGFP module⁶⁷ (adapted from Patriarchi *et al.*, Science, 2018)

GPCR activation leads to the closed state of cpGFP, which is bright due to restoration of the β -barrel (Figure 2.7).

2.7. Cell culture and transient transfection

HEK293T cells were cultured in DMEM supplemented with 10% fetal calf serum, L-glutamine, penicillin (100 U/ml) and streptomycin (100 μ g/ml) at 37°C and 7% CO₂. For FRET experiments, cells were seeded onto poly-D-lysine-coated UV-transparent quartz coverslips in 6-well plates 12-16 h before transfection. Cells were transfected using Effectene according to the manufacturer's instructions. cDNA amounts were 150 ng of each protomer of the wildtype and mutant *E*-sensors and 150 ng of the wildtype and mutant *A*-sensors per coverslip. In order to minimize glutamate contact with receptors, cell culture medium was exchanged for DMEM-GlutaMAX 24 h after transfection. Approximately 60 h after transfection, cells were washed twice with HBSS (150 mM

NaCl, 2.5 mM KCl, 2 mM MgCl₂, 4 mM CaCl₂, 10 mM HEPES, 10 mM glucose; pH 7.4) and incubated in HBSS buffer supplemented with 1.75 U/ml glutamate-pyruvate transaminase, 4 mM sodium pyruvate, and 0.1% BSA for 1 hour.

2.8. Uncaging experiments

To permit the detection of maximal activation speeds, we developed and employed synchronous activation of receptors by UV-light-triggered uncaging of an inactive caged glutamate derivative to rapidly release active glutamate onto intact cells. To synchronously photo-activate the mGluR1, we used a photolabile caged analog of glutamate, 4-methoxy-7-nitroindolinyl (MNI)-glutamate⁶⁸ (Figure 2.8).

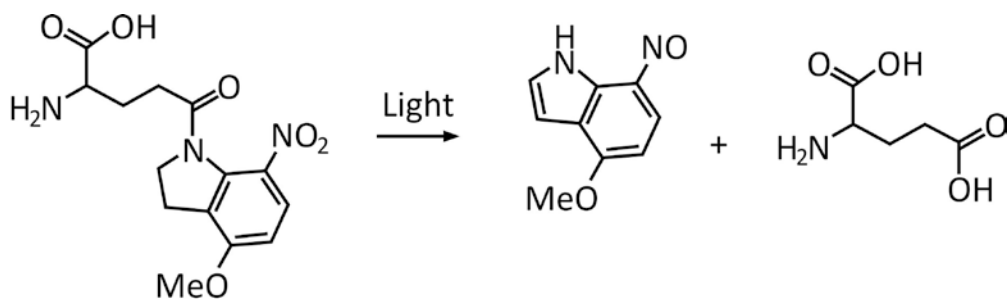


Figure 2.8. Photoinduced release of glutamate from MNI-caged-glutamate.

For FRET experiments, coverslips with sensors-expressing cells were mounted in an experimental chamber and placed on a custom-built inverted microscope, kept at room temperature, equipped with an oil-immersion objective Fluar 100x/1.30 Oil UV and a light-emitting diodes system pE-4000 as an excitation light source (Figure 2.9). Upon excitation of eCFP with 435 nm diode, fluorescence emission was simultaneously recorded at 483 ± 16 nm (CFP) and 535 ± 15 nm (YFP) before and after the addition of MNI-caged-*L*-glutamate (Figure 2.10). Fluorescence signals were

detected by photometry systems, each of which contained a gated photomultiplier (PMT) and photometer amplifier unit. Photocurrents were digitized at 10 kHz sampling frequency using an analog-digital converter and recorded with the pClamp software.

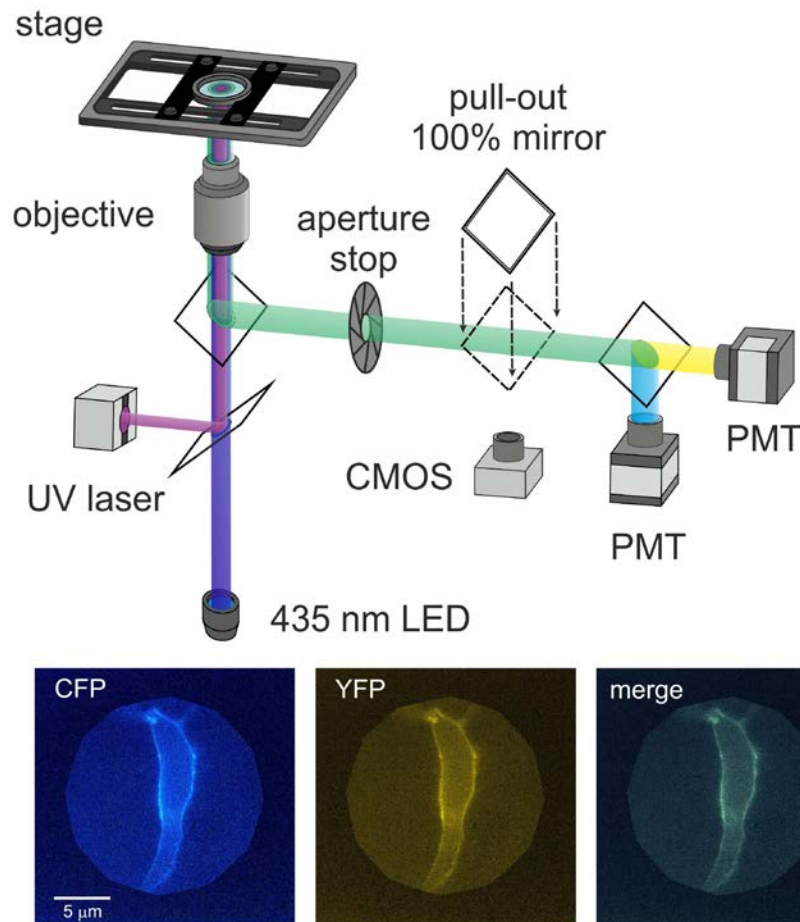


Figure 2.9. Schematic diagram of the custom built microscope setup for UV-uncaging studies. 435 nm LED excites the FRET donor CFP. Fluorescent light coming from the donor eCFP and the acceptor eYFP was either imaged with a CMOS camera, or split at 509 nm and collected by PMTs. In addition, the UV laser delivers a beam onto the specimen to uncage the ligand. A 405 nm edge filter blocks UV light in the emission path. Below are the images of the mGluR1 *E*-sensor expressed in a HEK293T cell.

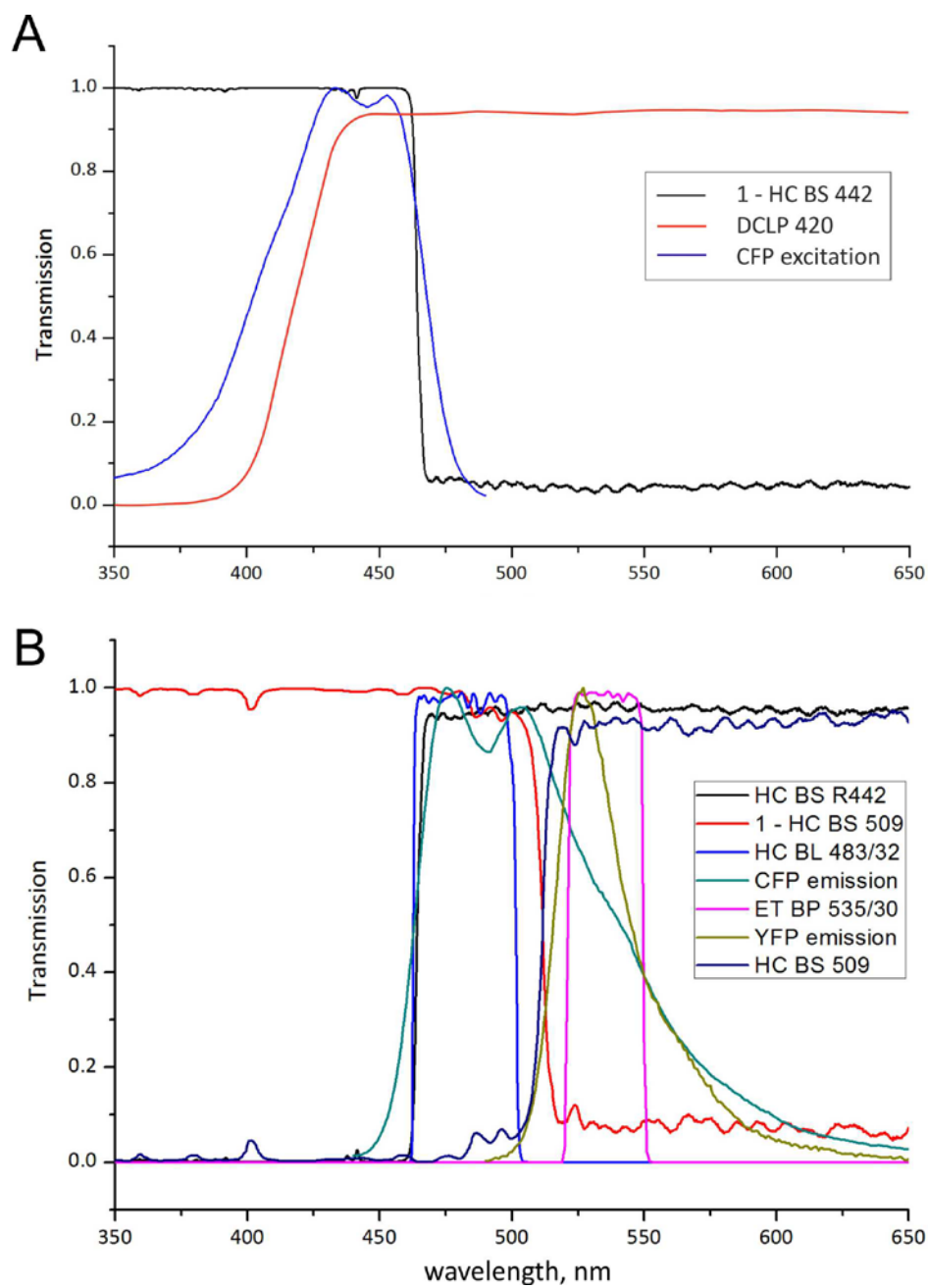


Figure 2.10. Optics in the microscope setup for ligand uncaging. Optical spectra in the excitation (A) and emission (B) light pathway overlaid with excitation and emission spectra of FRET donor and acceptor.

2.9. Fast epifluorescent imaging

Fast imaging was performed on the pre-assembled epifluorescent inverted microscope with customized optics (Figure 2.11). Chamber with sensors-expressing cells was placed on the microscope equipped with an oil-immersion objective HC PL APO 63× and xenon lamp coupled to a continuously tunable high speed polychromator.

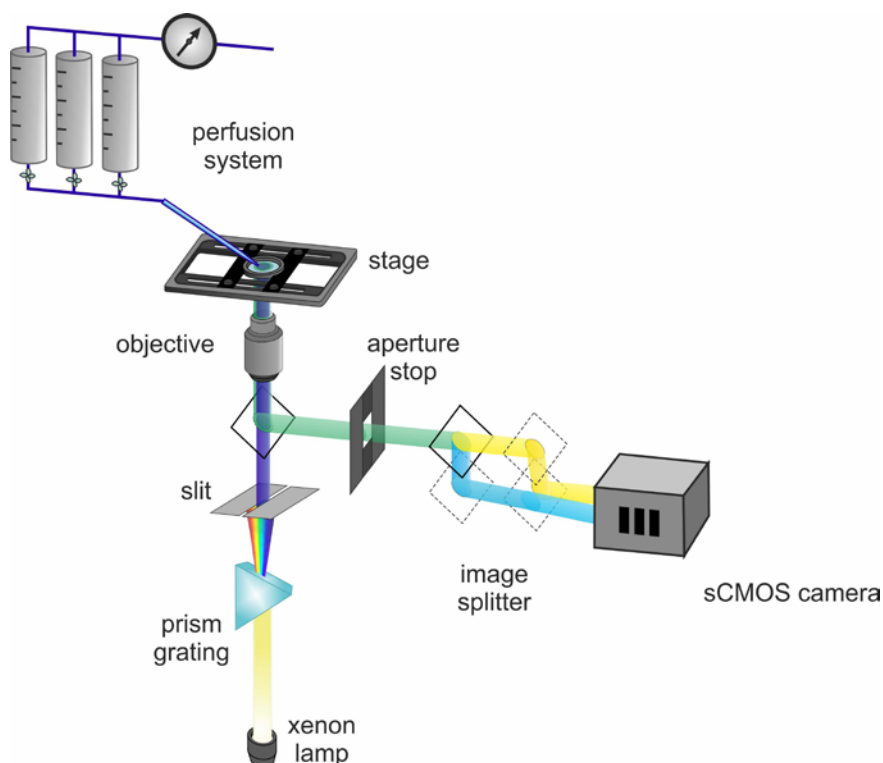


Figure 2.11. Schematic diagram of the microscope setup for fast imaging.

For FRET experiments, upon 10 ms excitation with 445 nm, fluorescence emission was simultaneously recorded at 470 ± 12 nm (CFP) and 535 ± 15 nm (YFP). In case of cpGFP-based receptor-sensors, upon 10 ms excitation with 483 nm, emission was recorded at 520 ± 17 nm. Fluorescence changes in cell membranes were detected by back-illuminated sCMOS camera using a dual image splitter, which was set to bypass mode for single-color sensors. Image sequences had

10 ms acquisition intervals and were recorded with the VisiView 4.0 software (Visitron Systems GmbH). Ligand application was performed using solenoid valves perfusion system with a 200 μm inner diameter manifold-tip.

2.10. Microplate photometry

FRET experiments in high-throughput format were done with a Synergy Neo2 Multi-Mode Reader. 24 hours after transfection HEK293T cells were resuspended in fresh DMEM and counted. At the density of $\sim 35,000$ cells/well cells were transferred to 96-well F-bottom plates. Fluorescence recordings were done 24 hours after the transfer. During the measurements cell were kept inside of the reader at 37 °C and 7% CO₂. YFP/CFP time courses were obtained through reader's ratiometric presets. HTRF-IP1 assay was performed using Tb²⁺-cryptate kit from Cisbio and standard ratiometric presets of the plate reader. In detail, excitation wavelength was set to 340 nm, emission channels were 620/665 nm, readout delay was set to 150 μs , data time collection was 500 μs and read height to 5 mm.

2.11. Photoswitching

In all experiments the pE4000 diodes system photoswitched SPA025. Particularly, we used 385 nm, 405 nm, 500 nm and 525 nm diodes, which were coupled to the collimator through liquid light guide. Collimator with aspheric condenser lens ($\text{\O}50$ mm, $f=40$ mm, $\text{NA}=0.60$, ARC: 350-700 nm) provided sufficiently even illumination of SPA025-1 solution in HBSS.

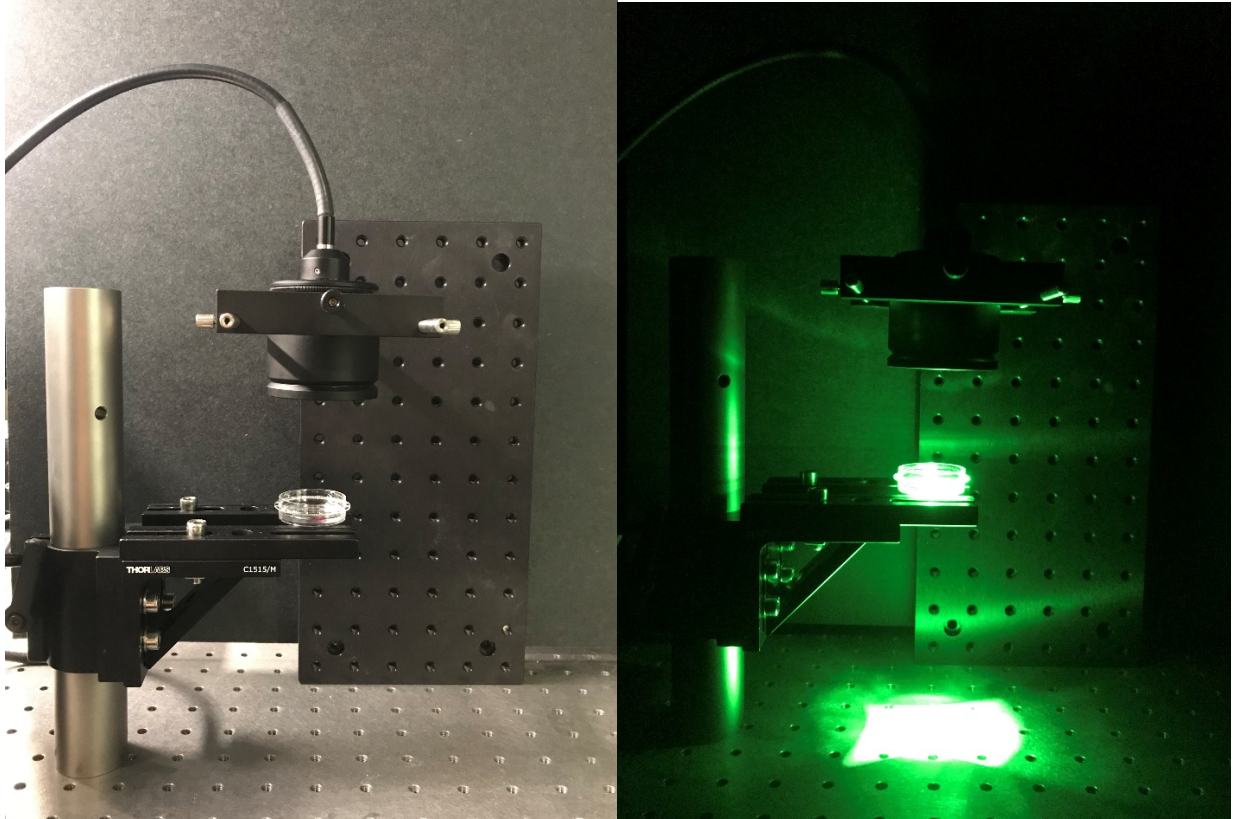


Figure 2.12. Illumination of a Petri dish with SPA025-containing solution using 505 nm diode.

3. RESULTS

3.1. mGluR1 activation kinetics

Photo-uncaging of MNI-caged-*L*-glutamate was achieved by a short 375 nm laser generated by a TTL controlled UV laser source. The laser was coupled to the microscope *via* a $\phi 105 \mu\text{m}$ quartz fiber optic light guide and collimated to the objective. To estimate the size of UV laser focal spot size we used caged fluorescein. A thin layer of CMNB-fluorescein was laid on a quartz coverslip and allowed to dry, to minimize lateral diffusion of the dye. The size of the fluorescent spot was measured through the obtained image from CMOS camera. Intensity image was plotted in a 3D domain and, assuming that the laser beam has an ideal Gaussian intensity profile, we approximated it with a 2D Gaussian function (Figure 3.1A):

$$F = F_0 + A \cdot \exp \left(-\frac{1}{2} \left(\frac{x \cdot \cos(\theta) + y \cdot \sin(\theta) - x_c \cdot \cos(\theta) - y_c \cdot \sin(\theta)}{w_1} \right)^2 - \frac{1}{2} \left(\frac{-x \cdot \sin(\theta) + y \cdot \cos(\theta) + x_c \cdot \sin(\theta) - y_c \cdot \cos(\theta)}{w_2} \right)^2 \right)$$

where

F_0 – offset; A – amplitude relatively to the baseline; x_c ; y_c – coordinates of the peak; w_1 and w_2 – x and y spreads of the blob respectively; θ – orientation of the blob.

Full width at the half-maximal values (*FWHM*) were further calculated as follows:

$$FWHM_x = 2w_1\sqrt{2\ln(2)}$$

$$FWHM_y = 2w_2\sqrt{2\ln(2)}$$

Radiant exposure measured after the objective was 458.6 J/cm^2 at 100% UV-laser power. Using caged fluorescein as a reference compound, we adjusted the laser power such that complete uncaging in this area was achieved well within a pulse duration of $300 \mu\text{s}$ (Figure 3.1B)

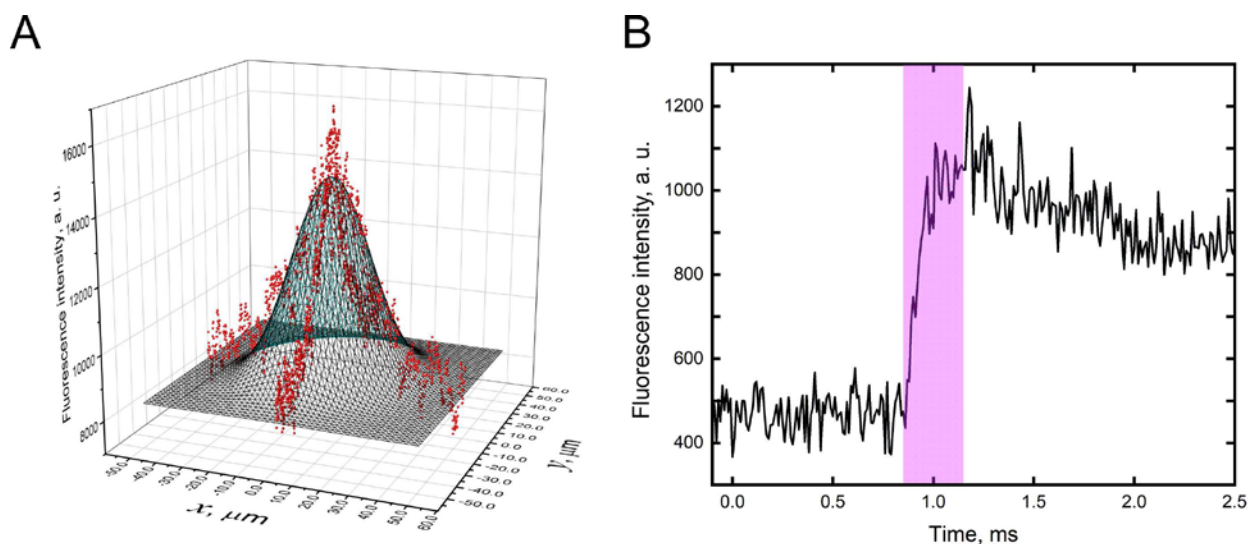


Figure 3.1. Spatio-temporal characteristics of uncaging. (A) Uncaging of fluorescein. x and y profiles through the fluorescence distribution F of uncaged CMNB-fluorescein were fitted with Gaussian functions spreading to half-maximal intensities $FWHM_x = 32.4 \pm 0.3 \mu\text{m}$ and $FWHM_y = 37.7 \pm 0.4 \mu\text{m}$. (B) Time course of fluorescence intensity of uncaged fluorescein upon laser illumination. Shown in pink is the $300 \mu\text{s}$ long UV-laser flash.

A kinetic model was derived from real-time FRET ratios (YFP/CFP). Fluorescence emissions of both donor and acceptor were corrected for background, fluorophores quenching, and bleedthrough of donor light into the acceptor channel essentially as described previously⁶⁹. In detail, background was measured in each channel for every experiment as a fluorescence intensity of neighboring non-transfected cells. Fluorophore quenching was corrected by subtracting the corresponding exponential curves for CFP and YFP, respectively. Bleedthrough of CFP emission

into the YFP channel was estimated as 36%. FRET ratios were further corrected for the transient inner filter effect of the nitrosoindole by-product of MNI-*L*-glutamate uncaging⁷⁰. A short-lived artefact was observed primarily in the CFP fluorescence channel, and was due to accumulation of the nitrosoindole by-product which absorbed light at ~410 nm. The fluorescence traces after photolysis were corrected by adding to the signal a rising exponential process with a rate constant of 40.2 ms starting at the time of the laser pulse, with an amplitude of 3% of the average CFP intensity and 0.5% of YFP intensity prior to uncaging. Corrected photocurrents were analyzed in OriginPro (OriginLab, USA).

FRET values were at time point *t* were determined as follows:

$$FRET = \left| \frac{R(t)}{R_a - R_b} \right|$$

where

R(t) is observed YFP/CFP ratio, *R_a* is a plateau ratio value at the peak of transient signal and *R_b* is a baseline ratio value before uncaging.

FRET time courses were fitted to the mono-exponential equation

$$FRET(t) = Ae^{-t/\tau}$$

where τ is the time constant and *A* is the amplitude of signal.

FRET in the mGluR1 *E*-sensor increased by 20-30% after the UV-pulse (Fig. 3.2A), which is compatible with the two protomers in the mGluR1 dimer moving towards each other, as seen in the inactive vs. active crystal structures of the mGluR1-VFT and, recently, of the full-length mGluR5

(PDB codes 1EWT/1EWK and 6N52/6N51, respectively)³⁹. In the case of the mGluR1 A-sensor, FRET decreased by about 5-15% (Fig. 3.2B); a similar decrease has been seen for essentially all analogous FRET-constructs reporting transmembrane conformational changes of GPCRs upon activation^{35,36}. This result is compatible with the notion of an outward movement of transmembrane domain VI upon activation²⁸⁻³⁰.

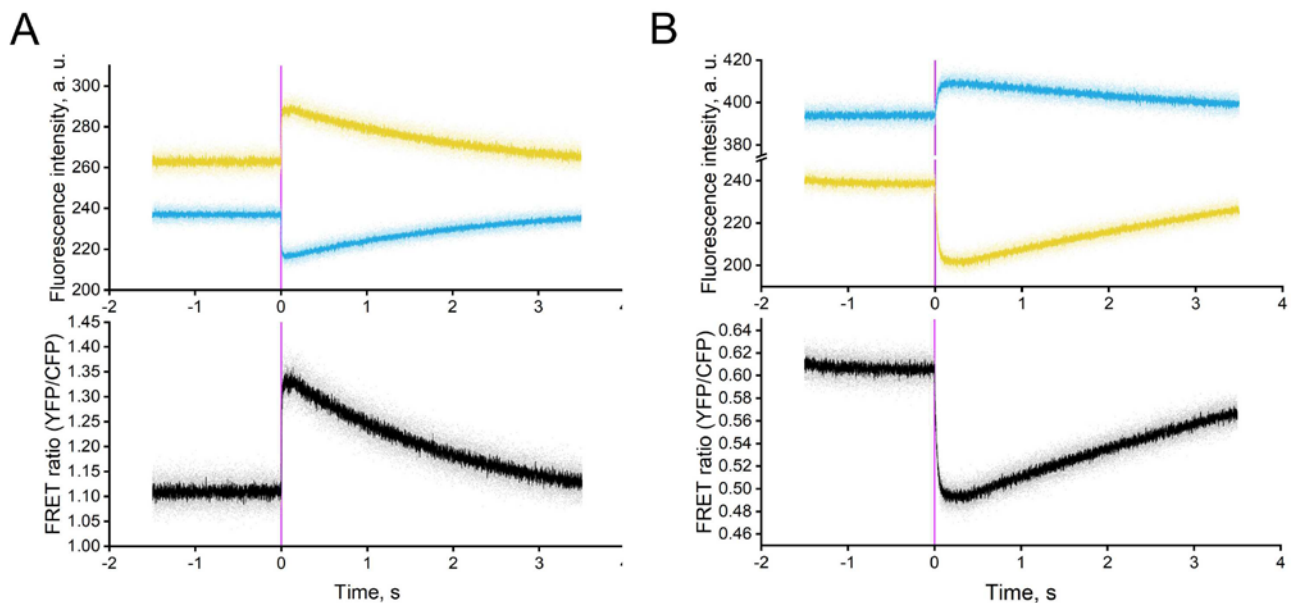


Figure 3.2. Activation of mGluR1 FRET sensors in living cells upon UV light-triggered uncaging of MNI-*L*-glutamate. Fluorescence emission intensities recorded in real-time in single intact cells expressing the *E*-sensor (A) or the *A*-sensor (B) before and after uncaging of 1 mM MNI-*L*-glutamate. Data collected from YFP, CFP and the corresponding corrected FRET ratio are depicted in yellow, blue and black, respectively. The transient nature of the signals is due to diffusion of uncaged glutamate away from the receptor.

The kinetics of these FRET changes, recorded with photomultipliers, were remarkably fast, with rise times of individual traces down to 1.2 ms (*E*-sensor) and 18.4 ms (*A*-sensor), and 1.9 ± 0.2 ms and 23.8 ± 0.7 ms for the corresponding averaged time courses (Figure 3.3). This is clearly faster than observed before using superfusion systems, which generated data in the order of ≈ 30 ms^{35,36}. The signals were transient, lasting for only a few seconds, compatible with the notion that the liberated glutamate dissipates in the solution after the UV-release.

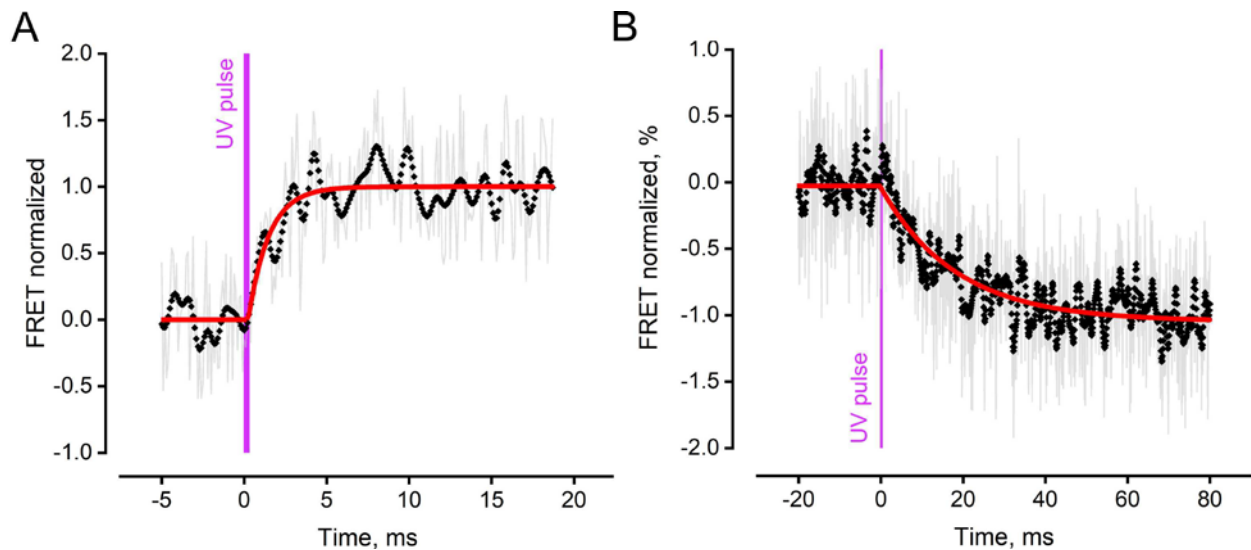


Figure 3.3. Millisecond kinetics of the *E*-sensor and the *A*-sensor activation. Shown are the normalized corrected FRET ratios of single cells expressing the *E*- (A) and *A*-sensor (B), respectively. The thickness of the purple line represents the duration of the UV pulse (300 μ s). Unfiltered ratio traces (shown in grey) were lowpassed at 1.25 kHz (black dots). The red curves represent monoexponential fits with time constants $\tau_{on}=1.2$ ms (A) and $\tau_{on}=18.4$ ms (B).

Low light intensities for photo-uncaging of MNI-glutamate resulted in slower activation kinetics, but the maximum speed was clearly reached at the higher light intensities and pulse durations used

(Figure 3.4), suggesting that the time courses shown in Figure 3.3 represents the maximal speed of the system.

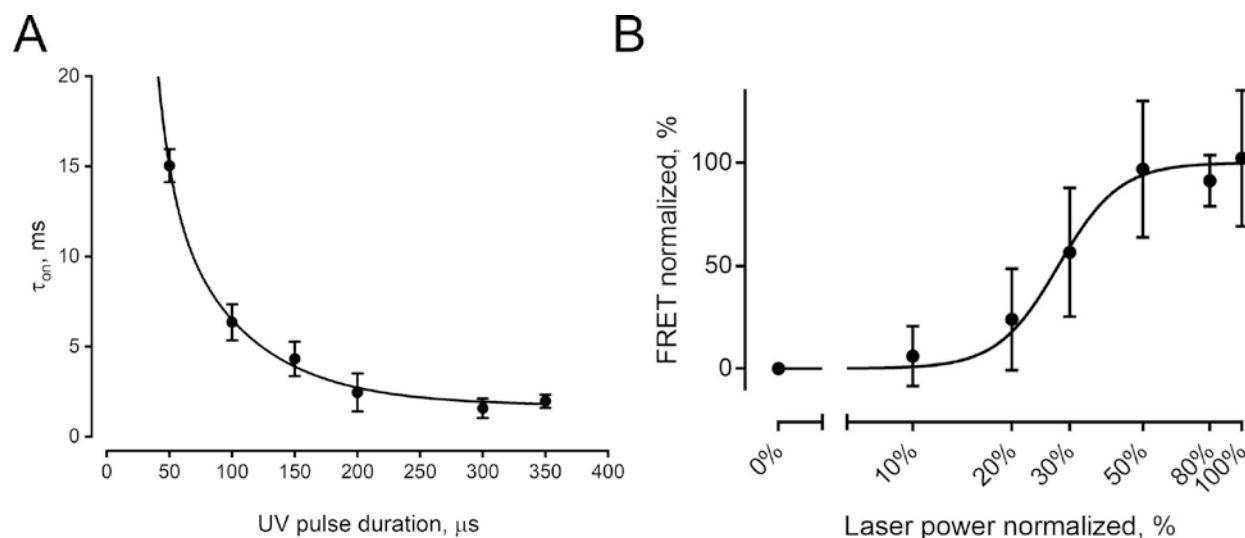


Figure 3.4. Dependence of mGluR1 *E*-sensor activation on UV-pulse duration and laser power.

(A) Time constant of the *E*-sensor as a function of UV flash duration. The data show that the rate constant approached a minimum when the flash duration was $>200 \mu$ s indicating the release of saturating concentrations of glutamate from MNI-glutamate. (B) Amplitude of the *E*-sensor FRET response as a function of UV-laser power with UV pulse duration set to 300μ s. Data points are mean \pm SEM from at least 4 different cells.

To verify that indeed these kinetics reflect inter- vs. intramolecular conformational changes in mGluR1, we made use of the C254E³⁹ mutant that disrupts communication from the N-terminal LB domain to the 7-TM domain in mGluR2 and 5 subtypes⁷¹. When this mutation was inserted into the *E*- and *A*-sensor of the mGluR1, this resulted in a moderate ($\approx 1/3$) loss of FRET-signal of the *E*-sensor (Fig. 2A), but a nearly complete loss ($\approx 90\%$) of the FRET signal of the *A*-sensor (Figure 3.5). This is compatible with the notion that the *A*-sensor reports essentially *intramolecular*

movements in the 7-TM domain, while the *E*-sensor reports largely (\approx two thirds of the FRET-signal) intermolecular movements of the protomers. With a rise time from averaged traces of 1.8 ± 0.2 ms, the kinetics of the FRET-signal in the C254E-mutated *E*-sensor were indistinguishable from the wild-type *E*-sensor (rise time 1.9 ± 0.2 ms). This further supports the notion that this is the speed of the intermolecular movements in the mGluR1 dimer. In Figure 3.5 we compare average FRET-signals of WT- (red) and C254E-mutated (blue) sensors induced by UV-light (300 μ s pulse) uncaging of 1 mM MNI-*L*-glutamate as in Figure 3.3.

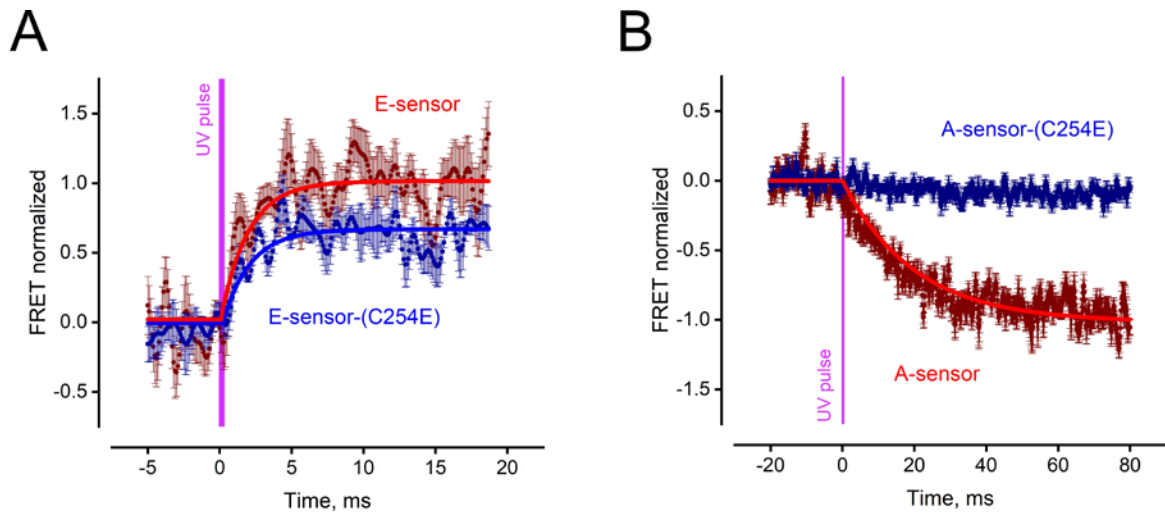


Figure 3.5. Effects of the C254E mutation on FRET-signals of the mGluR1 *E*- and *A*-sensors. (A) Activation of the *E*-sensor; fitting with a monoexponential function gave $\tau_{on}=1.9 \pm 0.2$ ms, $n=12$ (WT) and $\tau_{on}=1.8 \pm 0.2$ ms, $n=4$ (C254E); (B) Activation of the *A*-sensor; fitting with a monoexponential function gave 23.8 ± 0.7 , $n=8$ (WT); data for the C254E-mutated *A*-sensor could not be reliably fitted to a monoexponential function due to the essentially complete suppression of the signal amplitude. Mutant data were normalized to the maximum FRET response of wild-type *E*- (A) and *A*-sensor (B).

Using a glutamate uncaging that allows activation in the sub-millisecond range, we found that the first activation step, the rearrangement of the transmembrane domain of the two protomers within the receptor dimer, occurs within 1-2 ms (*E*-sensor). The coupling between this rapid rearrangement step and activation of the transmembrane domain is apparently loose, resulting in ≈ 20 -fold slower activation of the *A*-sensor.

3.2. mGluR1 photo-NAM.

To further tune light-controlled mGluR1 activity we used photoswitchable azobenzene compounds, analogs of the mGluR1 NAMs with high solubility in aqueous solutions. Synthesis and initial spectroscopic experiments were carried out in the Institute for Advanced Chemistry of Catalonia (iQAC-CSIC) under the supervision of Dr. Amadeu Llebaria, director of Medicinal Chemistry and Synthesis Group. As a reference NAM so called **Compound 6** was taken, which has already shown to act as a mGluR1 NAM and to inhibit uptake of mGluR1-specific ligands in rodent brain⁷². Azologization of the latter gave birth to a generation of photoswitchable compounds named SPA0XX. Among many, the most promising we find SPA025 and SPA025-HCl, the salt of the first product, obtained in order to enhance its solubility in aqueous solution (Figure 3.6).

If *trans* azobenzene is the active ligand, it exerts its effect on the receptor in the dark, and the ligand stops its influence on the receptor upon illumination with a suitable wavelength λ_1 that switches it to the inactive *cis* isomer. Restoration of the active state requires either a relaxation of azobenzene or illumination with a second suitable wavelength λ_2 . Such situation is defined as a *trans*-on compound.

On the other hand, if the *cis* azobenzene is the active ligand, while keeping the *trans* azobenzene in the dark, it has minimal or no effect on the receptor. Upon illumination with a suitable wavelength λ_1 that transforms *trans* to *cis* isomer, a gain of function of the ligand in the receptor is triggered. To go back to the initial state, it is required either a relaxation of azobenzene or illumination with a second wavelength λ_2 . This situation is defined as a *cis*-on compound.

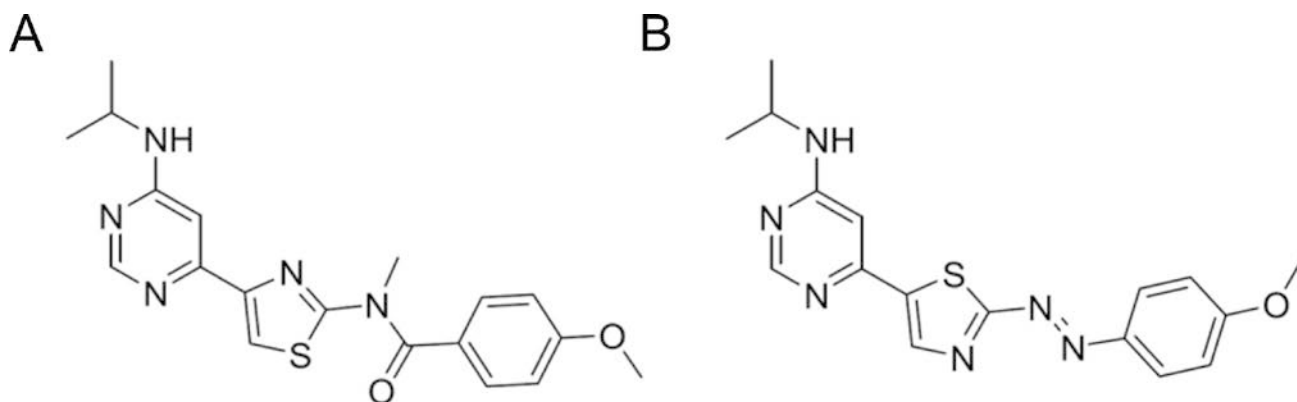


Figure 3.6. mGluR1 NAM. Compound 6 (left), and its photoswitchable analog – SPA025 (right).

To test photoswitching we measured the absorption spectra of both compounds in the dark, after illumination with UV light ($\lambda = 380$ nm) and after illumination with visible light of different wavelengths ($\lambda = 455/500/532/650$ nm) (Figure 3.7).

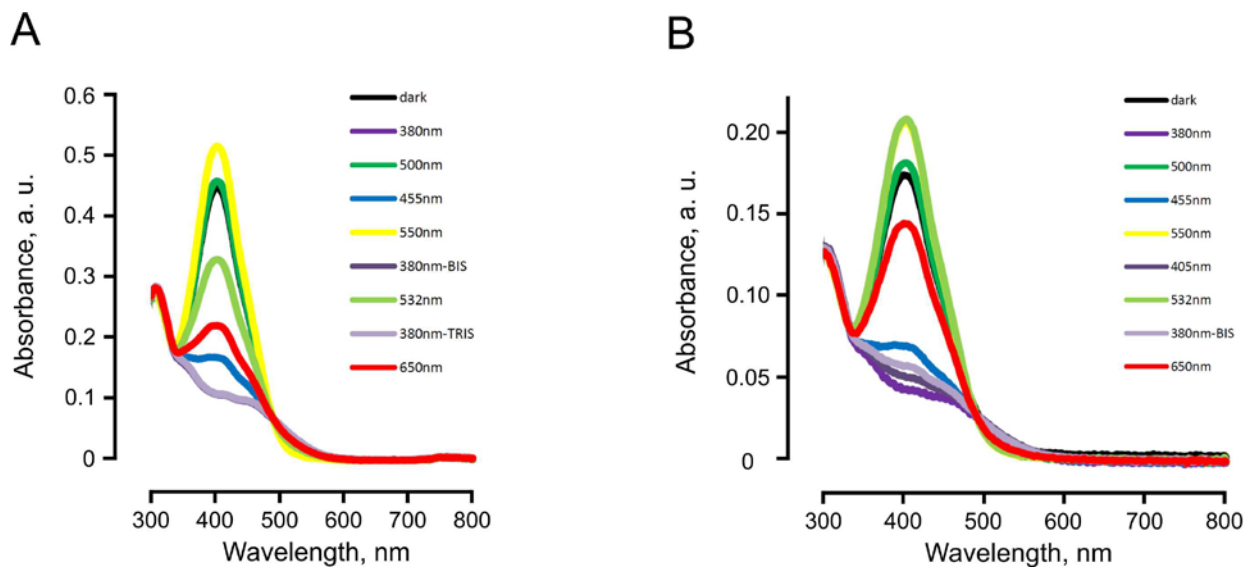


Figure 3.7. Photoisomerization of SPA025. Absorption spectra of SPA025 (A) and SPA025-HCl (B) under different illumination conditions

To study the activity of SPA025, we first used the previously described mGluR1 FRET A-sensor. Cells expressing the sensor were seeded in 96-well microtiter plates (Figure 3.8) and fluorescence time courses of CFP and YFP were read out to quantitatively evaluate the antagonistic activity of the SPA025 concentration series to glutamate.

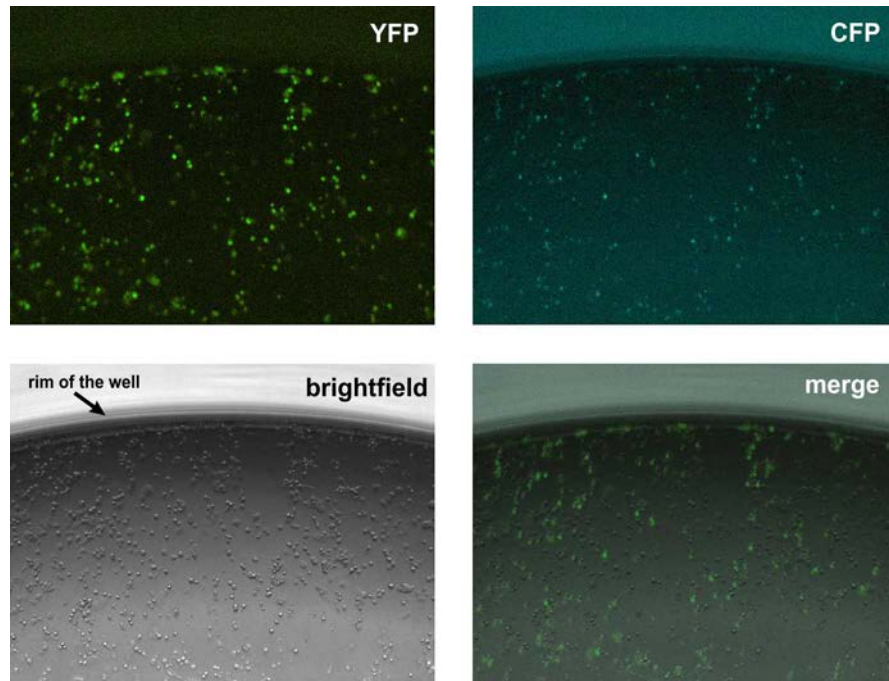


Figure 3.8. Wide-field images of HEK293T cells expressing mGluR1 intramolecular FRET-sensor on a bottom of microtiter plate. 10x magnification, dry immersion objective. Shown are fluorescent images of FRET acceptor and donor (YFP and CFP, respectively, top panels), brightfield and merged images (bottom panels).

Before adding to the cells, we kept SPA025 under light conditions similar to those used in above mentioned spectroscopic experiments. Microplate photometry showed that cells which were incubated with 500 nm illuminated SPA025 had significantly smaller FRET ratio change upon application of glutamate, than the cells incubated with 385 nm illuminated SPA025 (Figure 3.9).

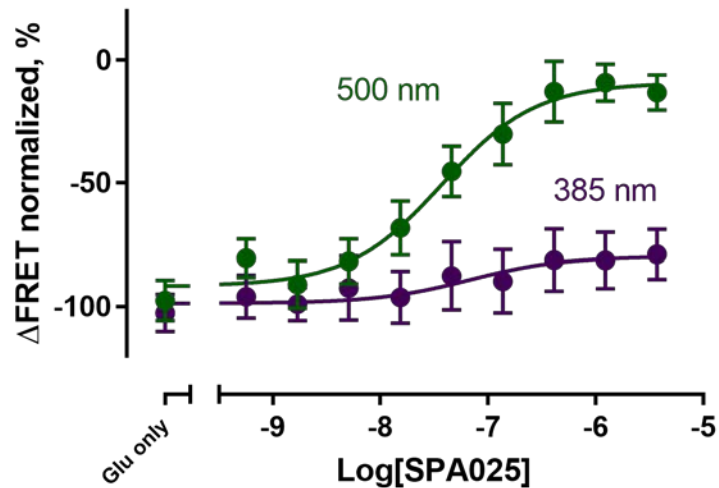


Figure 3.9. Quantification of SPA025 efficacy and affinity to mGluR1 in presence of 100 μM L-glutamate. Data shown are mean \pm SEM, $n = 7$. Data fitted with one-site association function ($EC_{50} = 37.4$ nM for *trans* and 67.0 nM for *cis* isomer)

Thus, we obtained azobenzene derivatives with a *trans*-on mGluR1 NAM activity. By means of incubation the cells with the ligand in the dark mGluR1 remains inactive. The illumination of the protein bound ligand with UV light isomerizes the azobenzene to the *cis* configuration, which triggers the receptor conformational evolution to a state that can be activated, provided that an orthosteric ligand is present. The recovery of the initial receptor inactive state can be achieved using a second wavelength (500-525 nm) for an effective transformation of the ligand to the *trans* isomer (Figure 3.10).

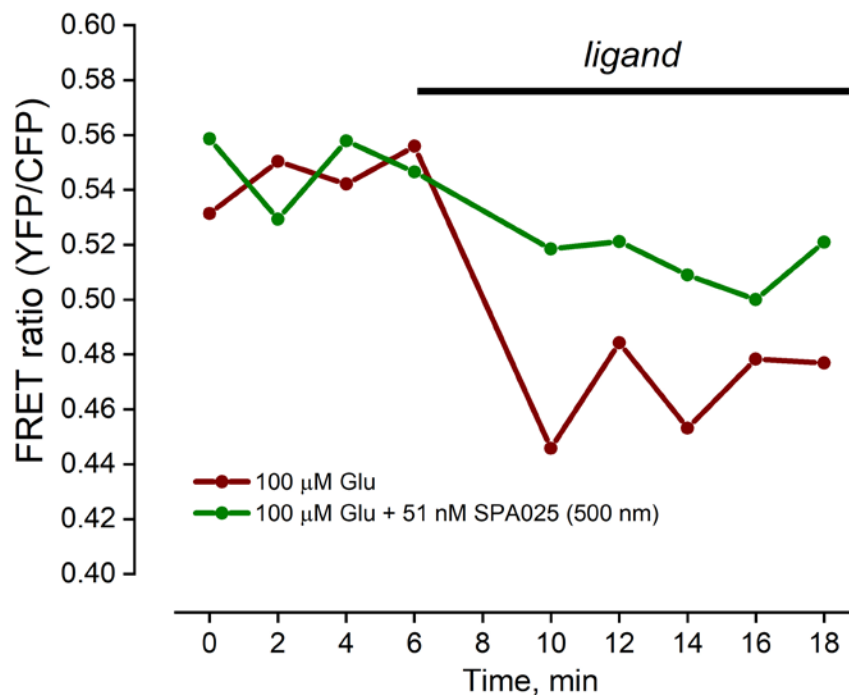


Figure 3.10. SPA025-dependent activation of mGluR1 upon L-glutamate stimulation.

Representative FRET ratio $R(t)$ traces of single wells (as shown in Figure 3.8). Fluorescence in each well comes from $\sim 35,000$ cells.

To evaluate the light-dependent effects of obtained photo-NAM on the downstream signaling, we used more soluble version SPA025-HCl for IP1 accumulation in mGluR1-WT-expressing cells. For each microplate four concentration-response curves were simultaneously generated, representing four different incubation conditions.

In this assay, the illumination with UV light (405 nm) induced a significant left shift of the concentration-response curve when compared to the non-illuminated control, compatible with a loss of the NAM potency of the *cis*-isomers (Figure 3.11).

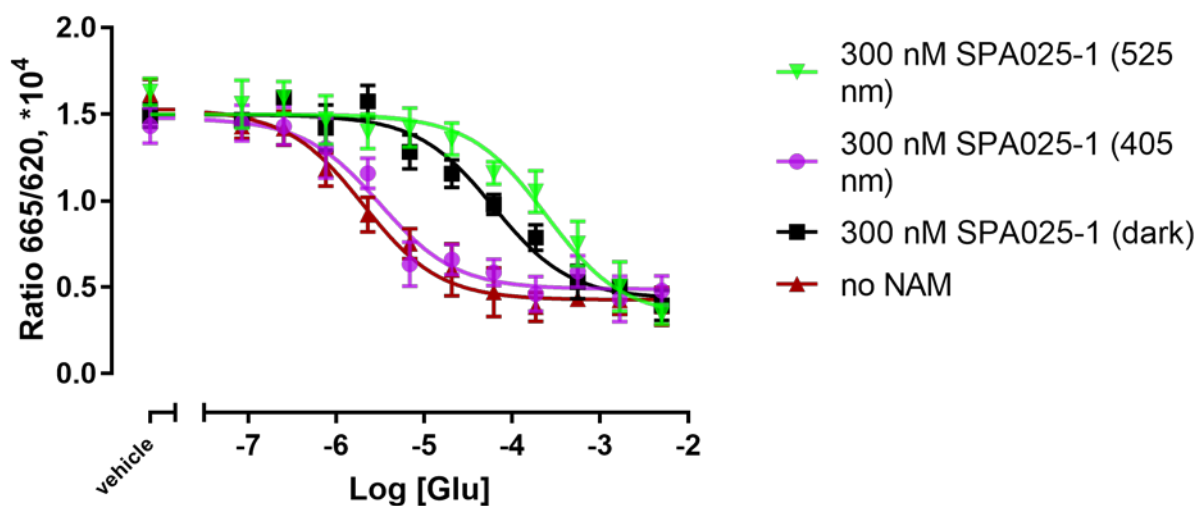


Figure 3.11. Concentration responses of SPA025-1 isomers on intracellular IP1 production measured using the HTRF-IP1 assay. Data are expressed as HTRF ratios and represent the mean \pm SEM from triplicate measurements in 2 independent experiments. Fitting resulted in

$$pEC50(405nm)=5.5, pEC50(525nm)=3.6, pEC50(dark)=4.2.$$

Illumination with green light (525 nm) brought the curves back to the right, indicating the restoration of the active state of the receptor. Thus, we observed photoinduced potency shift of SPA025-1 in the IP1 accumulation assay.

3.3. High-throughput spatially-resolved imaging of GPCR activation

To circumvent the limitations caused by ligand delivery speed in the context of GPCR activation kinetics measurements one could approach the problem from another end – by changing the way of signal detection. Instead of synchronizing the appearance of the agonist in the vicinity of every

receptor on the cell membrane we looked into regions of such size, where the temporal difference in arrival of the ligand to the opposite sides of them is insignificant.

In the beginning, we analyzed averaged fluorescent intensities of M3R-cpGFP upon ligand application over the whole cell (Figure 3.12A). Classically, this is done by averaging the intensity values of all pixels inside a user-defined polygon - region of interest (ROI₁). The time course in Figure 3.12B comes from the polygon ROI₁ in A. The inset curve was fitted to a monoexponential function with a rise time $\tau_{\text{cell}} = 41$ ms.

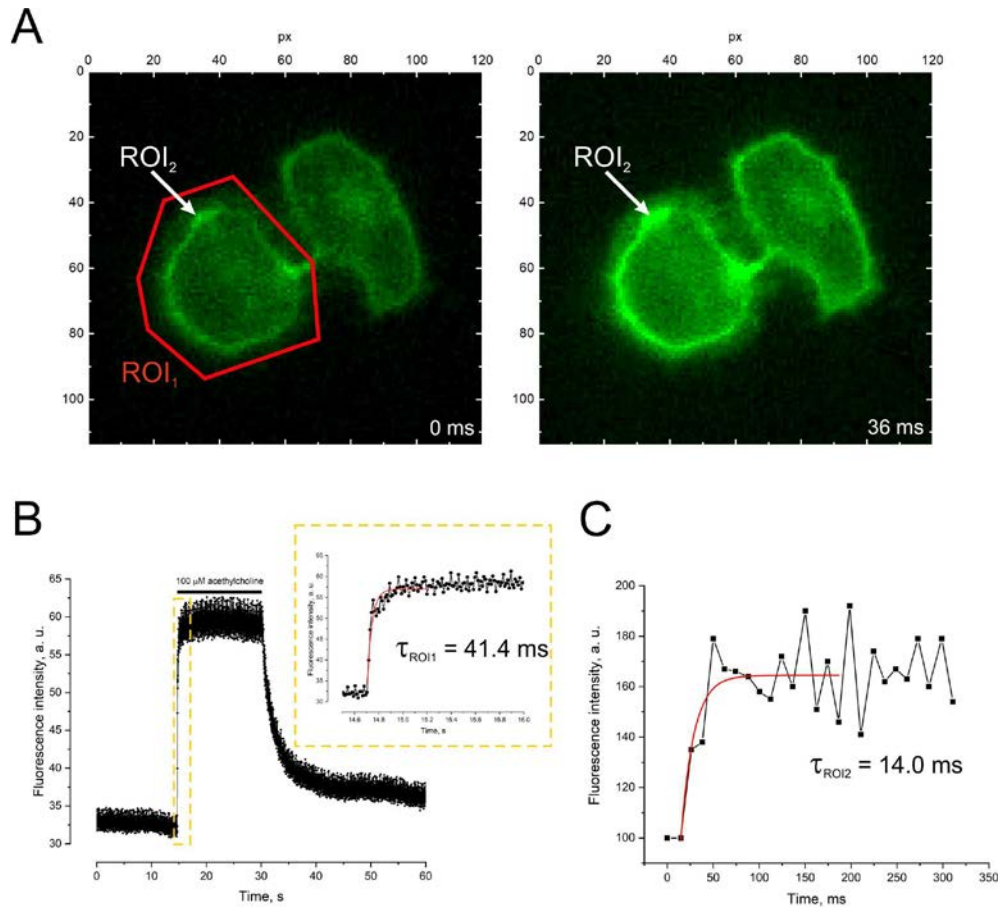


Figure 3.12. Activation of M3R-cpGFP. (A) Temporal image stacks obtained with sCMOS cameras at millisecond sampling intervals. Fluorescent intensity time courses of M3R-cpGFP upon acetylcholine stimulation averaged over ROI₁ (B) and ROI₂ (C).

However, fluorescent intensity time course of selected pixel (ROI₂, Figure 3.12A) rises faster upon ligand addition (Figure 3.12C). Since the focal volume in one single pixel is much smaller than the volume of an entire cell, kinetic-bias caused by ligand diffusion should become negligible. Here, mono-exponential fit results in an almost three times smaller rise time $\tau_{ROI} = 14$ ms.

Further spatio-temporal analysis of class A GPCRs activation confirmed gradual nature of cellular response, we observed that, for example, cellular membranes located closer to the perfusion tip were becoming active earlier than those ones further away when perfusion pressure was set lower (Figure 3.13).

This situation spurred the decision to develop a user-friendly framework for discovery of and sorting of activation heterogeneities. We set the image acquisition sampling to ~100 Hz before and after the addition of ligands. In order to improve signal-to-noise ratio, in some image sequences pixels were binned 2x2, and resulting intensity time courses of single pixels or bins in selected regions of interest were sorted by overall mean signal and dispersion, as a measure of the absolute receptor activation. Then, intensity time courses of each of such individual pixels or bins we fitted to the “plateau followed by monoexponential rise” equation:

$$F(t) = \begin{cases} F_0 & \text{for } t < t_0 \\ F_0 + A * \left(1 - e^{-\frac{t-t_0}{\tau_{on}}}\right) & \text{for } t \geq t_0 \end{cases}$$

where

F_0 – offset intensity before the application of the ligand;

A – amplitude of the signal upon ligand addition;

t_0 – starting time point of the response;

τ_{on} – rise time of the signal.

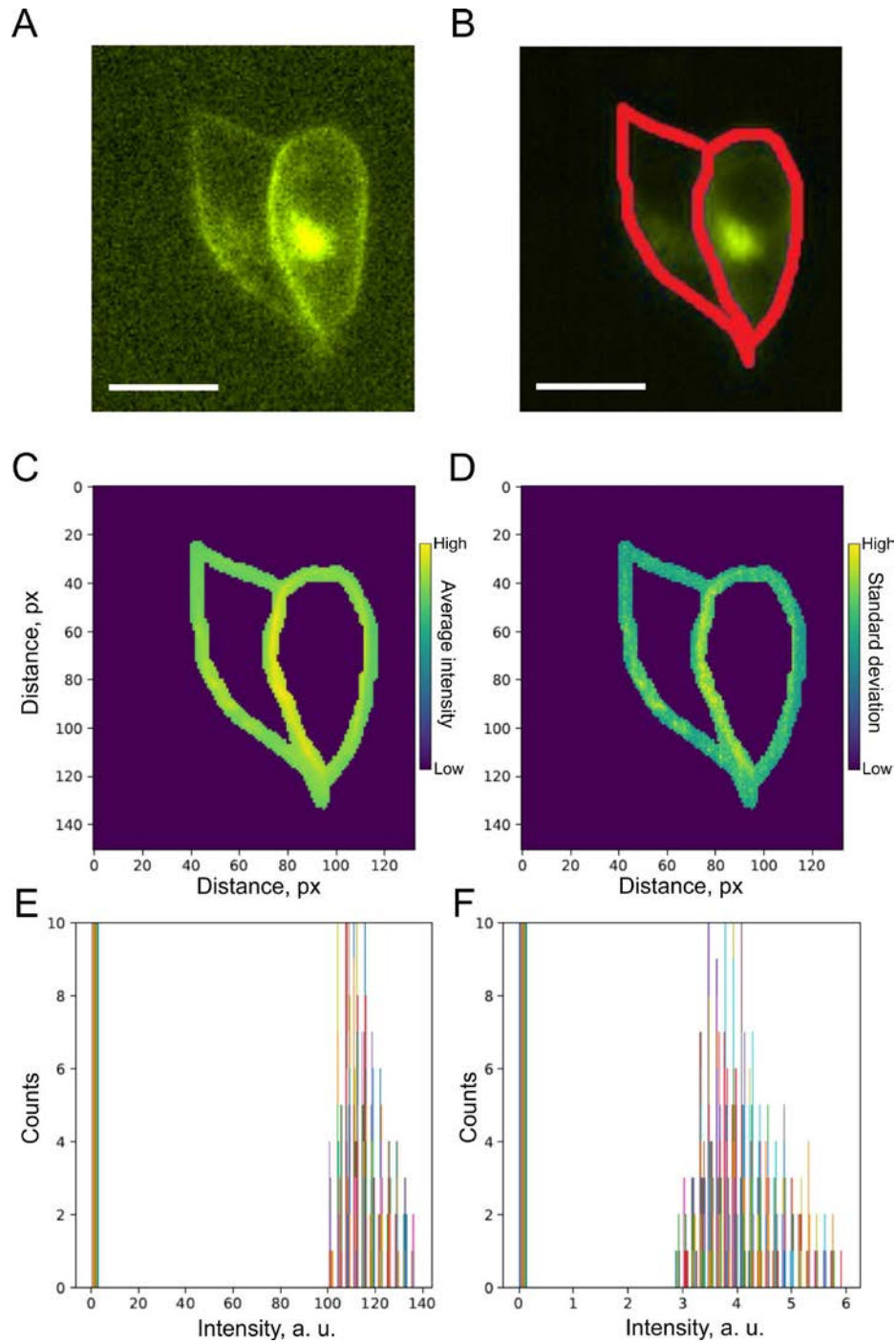


Figure 3.13. Workflow of single-pixel analysis of $\alpha 2aAR$ -cpGFP. (A) Wide-field images of HEK293T cells expressing $\alpha 2aAR$ -cpGFP. (B) User-defined ROI containing cellular membrane. Distributions of pixels over average intensity signal (C, E) and standard deviation (D, F), as a measure of receptor activation amplitude.

Three parameters were extracted from each fit, A , t_0 , τ_{on} , (Figure 3.14, *left*) and each pixel was then plotted in the 3D domain with indicated parameters as variables – “kinetic space” (Figure 3.14, *right*).

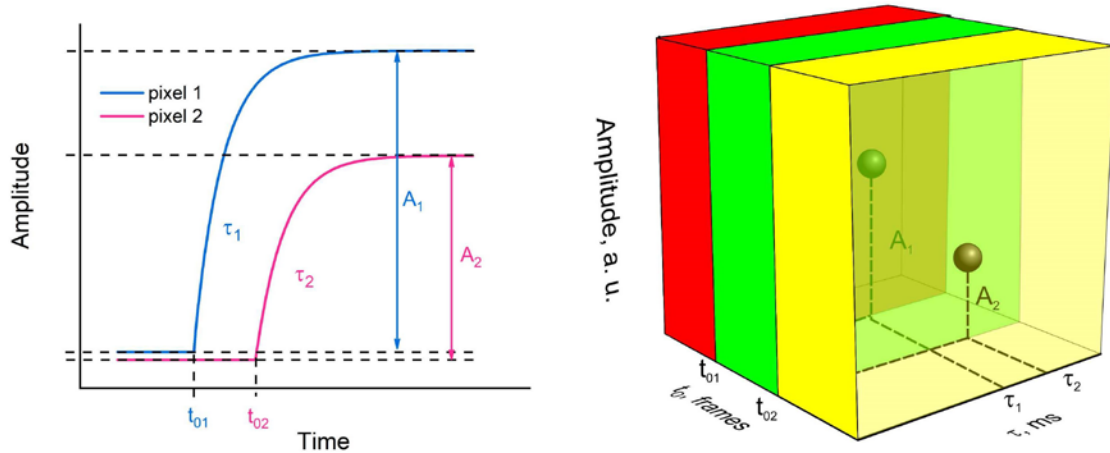


Figure 3.14. Schematics of the applied fit to each individual pixel during the kinetic analysis and extracted parameters (*left*) used as variables in “kinetic space” (*right*).

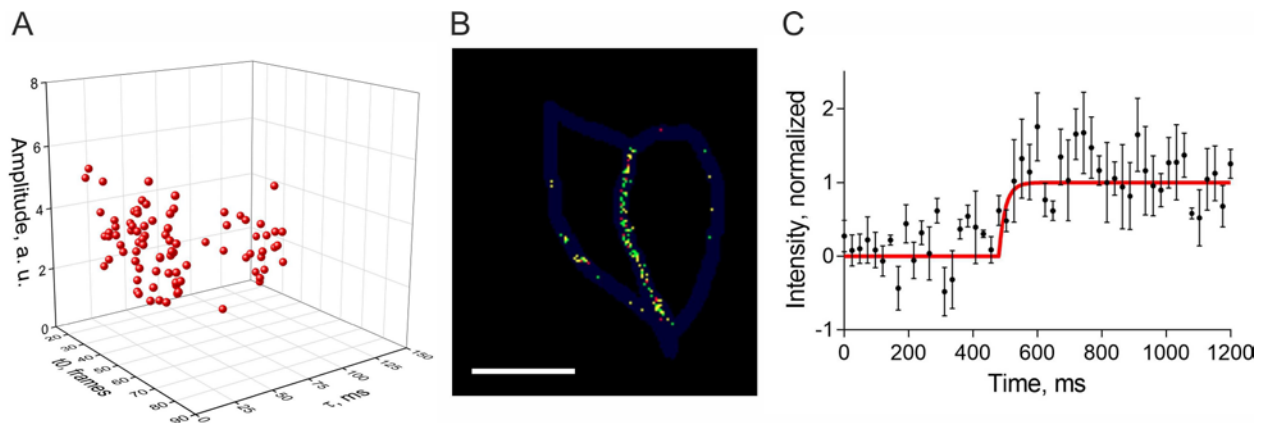


Figure 3.15. $\alpha_2\text{aAR}$ kinetic analysis of distinct pixels. (A) individual pixels plotted in kinetic space (B) activated pixels sorted by different starting point of the signal. Different colors represent time intervals of 200 ms (as in Figure 3.14, *right*). Scale bar is 5 μm . (C) Averaged kinetics of temporally aligned pixel traces upon 100 μM NE application. Data is mean \pm SD, $n = 4$. Red curve represents “plateau-monoexponential-rise” fit with a rise time of 14 ms.

Pixels could be afterwards sorted *ad lib* by any of the three above mentioned parameters to investigate certain patterns of GPCR activation (Figure 3.15).

To make sure that rise time obtained with this approach represents true activation kinetics we used again the mGluR1 A-sensor (Figure 3.16). Indeed, the fit resulted in essentially the same rise time as we have previously obtained using glutamate uncaging and PMT-based microscope.

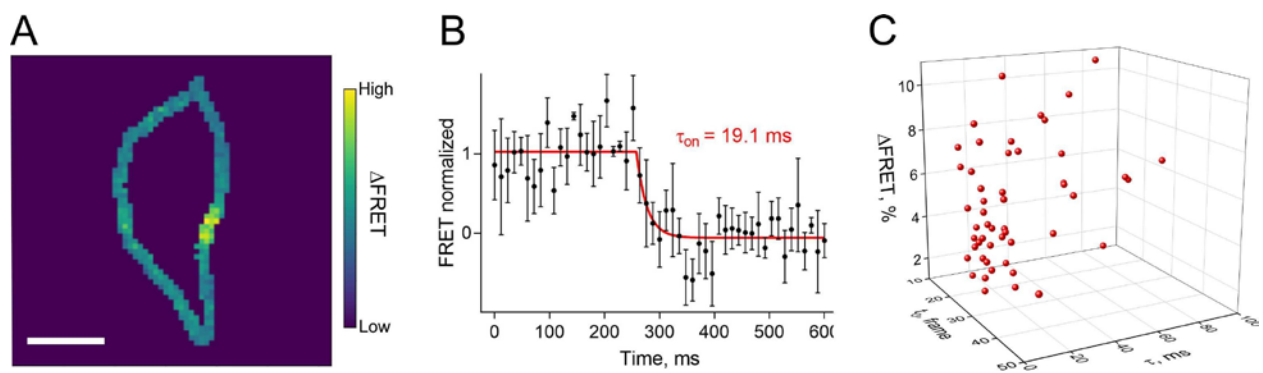


Figure 3.16. mGluR1 activation kinetics measured with single-pixel analysis. (A) Distributions of pixels over average Δ FRET signal, scale bar is 5 μ m. (B) Averaged kinetics of temporally aligned pixel traces upon 1 mM glutamate application. Red curve represents “plateau-monoexponential-rise” fit. Data are mean \pm SD, $n = 4$. (C) Individual pixels plotted in kinetic space

Similar results we also obtained for μ OR activation with morphine and DAMGO (Figure 3.17)

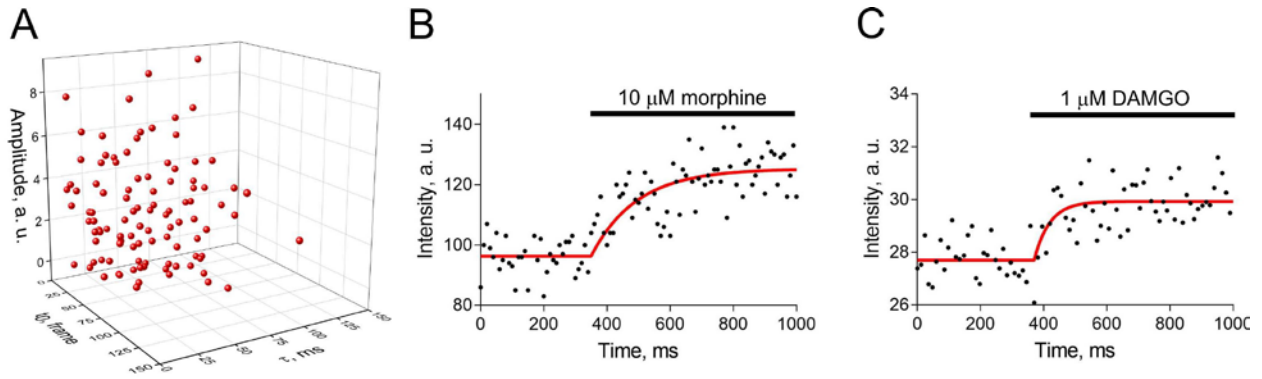


Figure 3.17. μ OR activation kinetics. (A) Individual pixels plotted in kinetic space. Activation of μ OR-cpGFP upon morphine (B) and DAMGO (C) application. Red curve represents “plateau-monoexponential-rise” fit.

When we observed the activation over the whole cell, we saw that the directional profile of activation is different from the direction of ligand application (Figure 3.18B), suggesting that the activation-profile is not just dictated by diffusion of the ligand, rather that there are allosteric effects on co-activation of individual receptors. This might occur direct via receptor-receptor interactions or indirectly by signaling partners, most likely G protein, β -arrestin or GRKs. Then looking at the activation over time we see that the rate of activation is faster than classical activation (Figure 3.19), which provides further evidence for a receptor co-activation in so called "signaling hotspots".

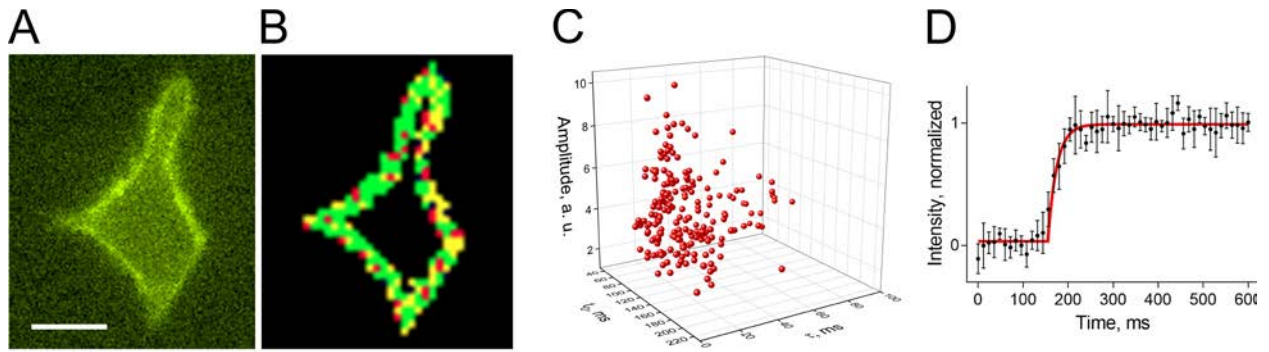


Figure 3.18. β 1AR activation kinetics. (A) Wide-field images of HEK293T cells expressing β 1AR-cpGFP, scale bar is 5 μ m. (B) Activated pixels sorted by different starting point of the signal. Different colors represent time intervals of 40 ms (as in Figure 3.14, *right*). (C) Individual pixels plotted in kinetic space. (D) Averaged kinetics of temporally aligned pixel traces upon 1 mM NE application. Data is mean \pm SD, $n = 4$. Red curve represents “plateau-monoexponential-rise” fit.

Clearly, the response displays a heterogeneous distribution along the cell-membrane, revealing distinct clusters of GPCR activation (Figure 3.18). This is the first evidence for the possible allosteric GPCR co-activation. Mathematically, this implies that the activation of GPCRs is not a sole function of the concentration (current understanding), but rather it is a function of the concentration and local density of activated receptors and the receptor environment (Figure 3.19).

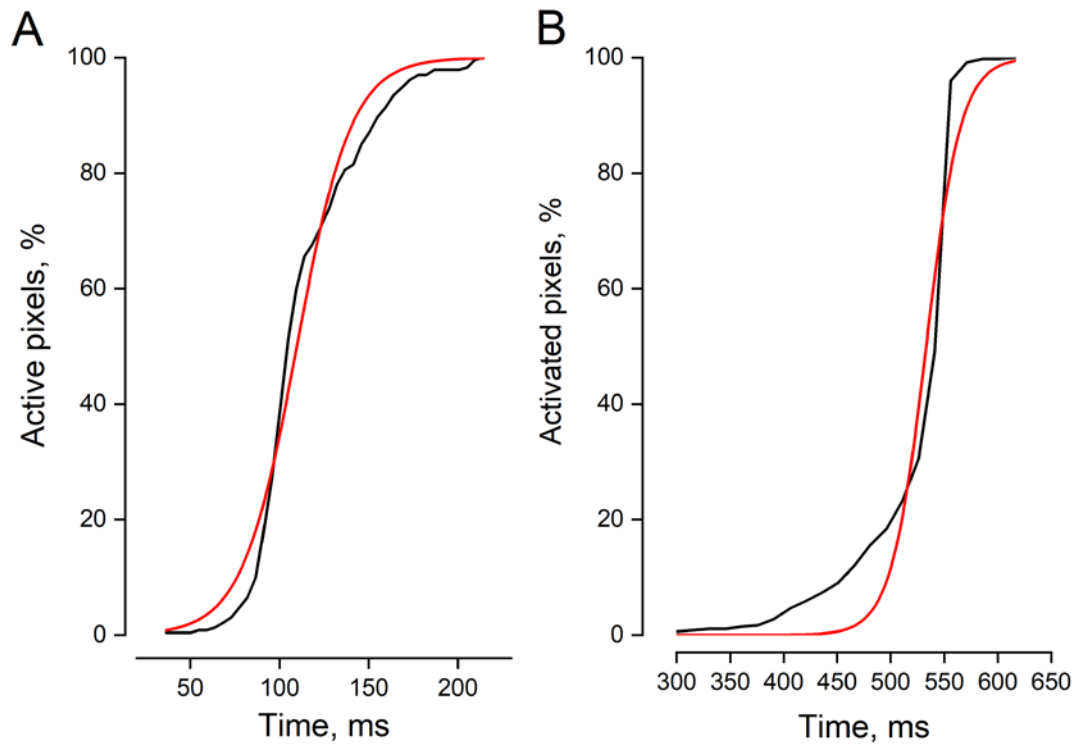


Figure 3.19. Whole cell GPCR activation deviates from receptor-concentration dependency. Pixel activation rate for β_1 AR (A) and α_2 aAR (B).

DISCUSSION

G-protein-coupled receptors form a family of signaling molecules in the membrane of cells that plays a key role in the transduction of cellular responses. Little is known how rapidly GPCRs can be activated. While the “light receptor” rhodopsin in the eye activates within 1 ms, all other GPCRs are thought to activate much slower. In this work several different approaches with advanced time resolution were used to activate and quantify the kinetics of dimeric metabotropic glutamate GPCR and several prototypical class A GPCRs.

The first part of this study reveals a number of novel findings about the kinetics of a class C GPCR, using the mGluR1 as an example. The whole cycle of activation and deactivation by a saturating agonist concentration is schematically summarized in Figure 6A, with the time constants of our measurements indicated. Using a technique that allows activation in the sub-millisecond range, we find that the first major activation step, the rearrangement of the transmembrane domain of the two protomers within the receptor dimer, occurs within 1-2 ms. This step is most likely preceded by agonist-induced closure of the ligand binding Venus Flytrap Domain, which mGluRs share with ionotropic receptors^{10,73}, and which has been shown in single molecule experiments with the isolated domains as well as in functional experiments to switch with sub-millisecond kinetics, i.e. faster than the dimer rearrangement that we observed. The loss of concentration dependence of activation at high ligand concentrations shows that the observed timescale indeed reports the speed of a conformational rearrangement of the dimer and not of diffusion or binding dynamics at the VFT domain. This rearrangement within another mGluR, the mGluR5, has very recently been characterized structurally by cryo-EM and crystallography⁴¹. These data suggest that closure of the VFT domain is intricately linked with a major rearrangement of the entire dimer, which also

involves a repositioning of the transmembrane (7-TM) domains, which rotate and come closer relative to each other. It is entirely plausible that this is what the *E*-sensor indicates.

The coupling between this rapid re-arrangement step and activation of the transmembrane (7-TM) domain is apparently loose, resulting in ≈ 20 -fold slower activation of the *A*- vs. the *E*-sensor. Loose coupling between initial and later steps in the agonist-induced activation of class A GPCRs has been suggested by NMR structural studies³² as well as molecular dynamics simulations, and it appears that the same is true for activation of class C GPCRs via their Venus Flytrap Domain. In complementary experiments, which were published⁷⁴ along with the uncaging data, it has been shown that not only activation but also deactivation is much slower for the *A*- than the *E*-sensor. As a consequence, the reaction scheme in Figure 3.20 indicates that in addition to the unliganded inactive (top left) and the double-liganded active states (bottom right), there are two metastable intermediate states, where either only the re-arrangement (top right) or the 7TM-conformation (bottom left) correspond to the fully active state. The roles and signaling properties of these intermediate states remain to be elucidated.

In recent biophysical studies on purified GPCRs the fully active state of the receptor was only obtained in the presence of other proteins that stabilized it, i.e. a G protein, a β -arrestin or a corresponding nanobody^{29,32,75,76}. This state was, therefore, not seen in the recent structural analysis of mGluR5 activation. Because of high intracellular levels of GTP this fully active state is presumably only transient in intact cells, and it is possible that it may not or only in part correspond to the active state reported here.

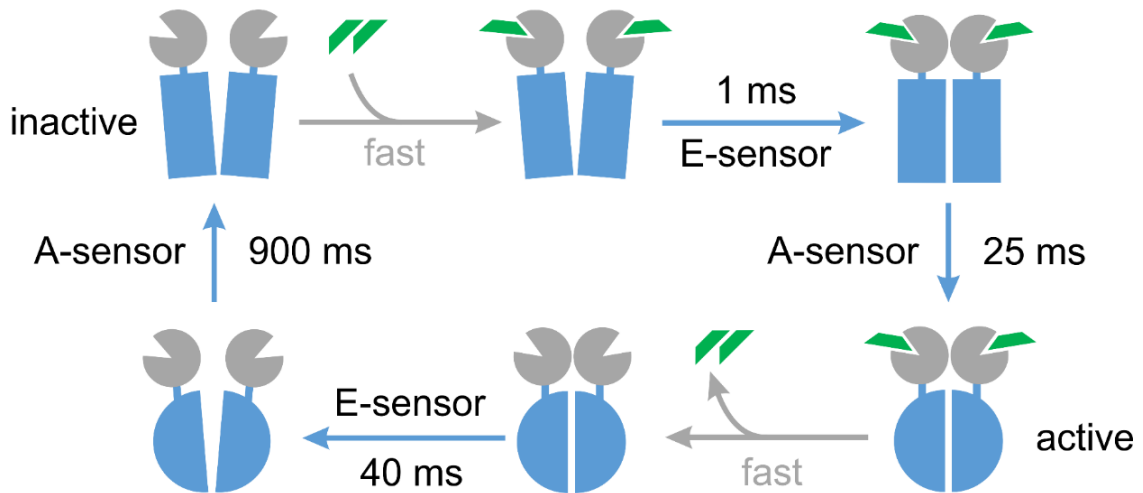


Figure 3.20. Schematic illustration of the activation and deactivation kinetics in mGluR1s. The glutamate ligands are indicated in green. The specified times are the time constants determined by the fits. It is assumed that the ligand binding is not rate limiting, i.e. that the ligand concentration is sufficiently high, and that ligand binding and closure of the Venus Flytrap Domain occur at sub-millisecond speed (“fast”).

Taken together, our data indicate that TM domain activation of the mGluR1 begins with a conformational change in the receptor dimer that lasts only about 1 ms. However, in contrast to rhodopsin activation, where the active meta-II state of the transmembrane domain is achieved in 1 ms, achievement of the fully active conformation of the mGluR1 in the 7TM domain then takes much longer (≈ 20 ms), indicating loose coupling between the two processes. Likewise, the return to the inactive state occurs stepwise, first in the dimer rearrangement and then in the 7-TM domain. The signaling competence of the resulting intermediate states remains to be identified. This stepwise process of activation and deactivation may contribute to flexibility and in the receptors’ ability to trigger downstream signals.

In the second part of this study we validated the newly obtained azobenzene-based photoswitchable compounds SPA0XX as mGluR1 NAMs in pharmacological IP1 accumulation assay with mGluR1-WT expressed in cells. FRET-based activation sensors of mGluR1 allowed us to define a way to perform a fine control of receptor activity by tuning the wavelength of illumination between 385 and 525 nm. Concentration-response curves and their IC₅₀-values were obtained under different illumination conditions.

Such compounds can be used to effectively control temporal dosing patterns with light in biological systems, for example directly in the CNS. Photopharmacology has been proven to be a powerful tool for such tasks since it enables the spatio-temporal control of target proteins with light-controlled receptor-specific drugs. Particularly, light can stop the drug action and enable accurate dosing patterns that can be adjusted in real-time⁷⁷.

In recent studies from our lab it has been shown that GPCR activation and signaling exhibits a certain compartmentalization, as in cell surface hotspots⁷⁸. This raised the immediate follow-up question if receptor activation occurs homogeneously or is following a certain heterogeneity along a cell membrane, which we investigated in the third chapter of this study. Better understanding where and how these activation and deactivation processes are taking place has a significant biological impact for therapeutic implications, selective drug targeting, as well as drug discovery. To date, we are lacking a holistic mathematical understanding/model on how these processes are driven.

We already obtained data, which provides good evidence of such heterogeneity for several typical class A GPCRs, and set up a pipeline for image-based kinetic analysis. Our kinetic assays are based on fluorescence microscopy and rely on a new concept of GPCR sensors, reporting the conformational changes of GPCR activation due to the insertion of circular permuted green

fluorescent proteins^{66,67}. We have also shown that our newly developed assay reports the same activation kinetics of mGluR1 as our rapid uncaging experiments. In such a kinetic assay, sCMOS cameras obtain temporal image stacks of cells expressing GPCR activation. Stacks are sampled at milliseconds intervals while concurrently applying receptor ligands.

Besides confirming activation kinetics of mGluR1, we measured rise times for several class A GPCRs, including M₃R, α_{2A} AR, β_1 AR and μ OR. We further developed a user-friendly algorithm to search for activation heterogeneities using both single- and dual-color sensors. Using our approach, we noticed that the amplitude of GPCR activation signal is not only dependent on the amount of activated receptors, but also has some level of correlation with the local density of activated receptors.

In terms of the mechanisms of receptor activation one of the possible biological implications of our results could be that receptors on the cell surface try multiple times to move into an active conformation, and because of a certain receptor “floppiness” combined with relatively high energy barriers, we observe such spread in receptor activation starting points and rise times. In terms of signaling biology such scatter across the cellular membrane might be one of the prerequisites for compartmentalized intracellular signaling. Potentially, these findings combined with a thorough drug screening a deeper understanding of this cardiac disease and facilitate the development of new therapeutic strategies. As we cannot probe the cell to a higher resolution; one must turn to mathematical modelling to test our hypothesis.

Future work in this direction will tell us not only how fast receptors get activated, but also where and when, and how their activation can be precisely controlled.

SUMMARY

G-protein-coupled receptors (GPCRs) are the largest family of membrane proteins that transmit both internal and external stimuli into the intracellular space and regulate a diverse spectrum of physiological processes in eukaryotic cells. Among the GPCRs, the “light receptor” rhodopsin has been shown to activate with a re-arrangement of the transmembrane helix bundle within ≈ 1 ms, while all other receptors are thought to become activate much slower, in subsecond range at saturating concentrations. Current work is focused on activation kinetics of a typical dimeric GPCR, the metabotropic glutamate receptor-1 (mGluR1), and several class A GPCRs, as muscarinic receptor 3 (M3R), adrenergic ($\alpha 2aAR$ and $\beta 1R$) and opioid (μOR) receptors. We first used UV-light-triggered uncaging of glutamate in intact cells. At saturating ligand concentrations the rearrangement between the mGluR1 subunits occurs at a speed of 1-2 ms. These changes were followed by significantly slower conformational changes in the transmembrane domain (20 ms). Second chapter of this work is dedicated to characterization of novel photoswitchable negative allosteric modulators for mGluR1, which under certain illumination conditions were shown to bind to its transmembrane core and block the conformational change as well as the downstream signaling. We also developed a framework for image-based kinetic analysis of GPCRs, which allowed us to measure activation kinetics of several prototypical class A GPCRs and to discover membrane heterogeneities of GPCR activation. Results of this work suggest that GPCR activation signal is not only dependent on the amount of activated receptors, but also has some level of correlation with the local density of activated receptors.

ZUSAMMENFASSUNG

G-Protein-gekoppelte Rezeptoren (GPCRs) sind die größte Familie der membranständigen Proteine, welche sowohl interne als auch externe Stimulationen in den intrazellulären Raum weiterleiten und somit in Eukaryonten ein breites Spektrum an physiologischen Prozessen regulieren.

Innerhalb der GPCRs konnte für den „Lichtrezeptor“ Rhodopsin gezeigt werden, dass dessen Aktivierung, welche eine räumliche Umorientierung der Transmembrandomänen beinhaltet, innerhalb von einer Millisekunde erfolgt, wohingegen angenommen wurde, dass die meisten anderen dieser Rezeptoren wesentlich langsamer, im Sekundenbereich, aktiviert werden.

Die vorliegende Arbeit ist auf die Aktivierungskinetiken eines typisch- dimerischen Rezeptors, nämlich dem metabotropischen Glutamat- rezeptor 1(mGluR1), sowie einige Klasse-A GPCRs fokussiert, darunter befinden sich sowohl der muskarinische M3-Rezeptor, die adrenergen α_2A - und β_1 -Rezeptoren als auch der μ -opioid Rezeptor.

Wir nutzten zunächst durch UV-Licht aktivierbares Glutamat auf intakten Zellen. Hierbei erfolgte, unter Verwendung von Sättigungskonzentrationen, die Umorganisation der mGluR1- Untereinheiten innerhalb von ein bis zwei Millisekunden. Diesen Änderungen folgte eine signifikant langsamere Konformationsänderung von 20 Millisekunden in den Transmembrandomänen.

Der zweite Teil dieser Arbeit befasst sich mit der Charakterisierung von neuen, durch Licht schaltbaren, negativen allosterischen Modulatoren des mGluR1-Rezeptors. Für diese konnte

gezeigt werden, dass sie unter bestimmten Belichtungsbedingungen im Mittelpunkt der Transmembrandomänen binden und dadurch sowohl die Konformationsänderung des Rezeptors als auch dessen weitere Signaltransduktion verhindern.

Zudem entwickelten wir ein Systemumfeld zur bildbasierten Analyse von GPCR-Kinetiken, welches es uns erlaubte die Aktivierungskinetiken einiger exemplarischer Klasse A GPCRs zu messen und heterogene Aktivierungskinetiken von GPCRs auf Zellmembranen zu entdecken.

Die Resultate dieser Arbeit legen nahe, dass Aktivierungs- Signale von GPCRs nicht nur von der Menge der aktivierten Rezeptoren abhängen, sondern zusätzlich auch zu einem gewissen Grad mit der lokalen Dichte von aktivierten Rezeptoren korrelieren.

REFERENCES

1. Pierce, K. L., Premont, R. T. & Lefkowitz, R. J. Seven-transmembrane receptors. *Nat. Rev. Mol. Cell Biol.* **3**, 639–650 (2002).
2. Wettschureck, N. & Offermanns, S. Mammalian G proteins and their cell type specific functions. *Physiol. Rev.* **85**, 1159–1204 (2005).
3. Lohse, M. J., Benovic, J. L., Codina, J., Caron, M. G. & Lefkowitz, R. J. I-Arrestin : A Protein That Regulates [I-Adrenergic. *Science (80-.)*. 1–4 (1984).
4. Kim, Y. M., Barak, L. S., Caron, M. G. & Benovic, J. L. Regulation of arrestin-3 phosphorylation by casein kinase II. *J. Biol. Chem.* **277**, 16837–16846 (2002).
5. Garland, S. L. Are GPCRs still a source of new targets? *J. Biomol. Screen.* **18**, 947–966 (2013).
6. Tesmer, J. J. G. Hitchhiking on the heptahelical highway: Structure and function of 7TM receptor complexes. *Nat. Rev. Mol. Cell Biol.* **17**, 439–450 (2016).
7. Weis, W. I. & Kobilka, B. K. The Molecular Basis of G Protein – Coupled Receptor Activation. (2018).
8. Fredriksson, R., Lagerström, M. C., Lundin, L. G. & Schiöth, H. B. The G-protein-coupled receptors in the human genome form five main families. Phylogenetic analysis, paralogon groups, and fingerprints. *Mol. Pharmacol.* **63**, 1256–1272 (2003).
9. Attwood, T. K. & Findlay, J. B. C. Design of a discriminating fingerprint for g-protein-coupled receptors. *Protein Eng. Des. Sel.* **6**, 167–176 (1993).

10. O'Hara, P. J. *et al.* The ligand-binding domain in metabotropic glutamate receptors is related to bacterial periplasmatic binding proteins. *Neuron* **11**, 41–52 (1993).
11. Romano, C., Yang, W. L. & O'Malley, K. L. Metabotropic glutamate receptor 5 is a disulfide-linked dimer. *J. Biol. Chem.* **271**, 28612–28616 (1996).
12. Ward, D. T., Brown, E. M. & Harris, H. W. Disulfide bonds in the extracellular calcium-polyvalent cation-sensing receptor correlate with dimer formation and its response to divalent cations in vitro. *J. Biol. Chem.* **273**, 14476–14483 (1998).
13. Pi, M. *et al.* Identification of a novel extracellular cation-sensing G-protein-coupled receptor. *J. Biol. Chem.* **280**, 40201–40209 (2005).
14. White, J. H. *et al.* Heterodimerization is required for the formation of a functional GABA(B) receptor. *Nature* **396**, 679–682 (1998).
15. Zhao, G. Q. *et al.* The receptors for mammalian sweet and umami taste. *Cell* **115**, 255–266 (2003).
16. Kniazeff, J. *et al.* Closed state of both binding domains of homodimeric mGlu receptors is required for full activity. *Nat. Struct. Mol. Biol.* **11**, 706–713 (2004).
17. Tehan, B. G., Bortolato, A., Blaney, F. E., Weir, M. P. & Mason, J. S. Unifying Family A GPCR Theories of Activation. *Pharmacol. Ther.* **143**, 51–60 (2014).
18. Thal, D. M., Glukhova, A., Sexton, P. M. & Christopoulos, A. Review Structural insights into G-protein- coupled receptor allostery. *Nature* (2018). doi:10.1038/s41586-018-0259-z
19. Yuan, S., Filipek, S., Palczewski, K. & Vogel, H. Activation of G-protein-coupled receptors correlates with the formation of a continuous internal water pathway. *Nat. Commun.* **5**, 1–10

- (2014).
20. Manglik, A. & Kobilka, B. The role of protein dynamics in GPCR function: Insights from the β 2AR and rhodopsin. *Curr. Opin. Cell Biol.* **27**, 136–143 (2014).
 21. Hofmann, K. P. *et al.* A G protein-coupled receptor at work: the rhodopsin model. *Trends Biochem. Sci.* **34**, 540–552 (2009).
 22. Knierim, B., Hofmann, K. P., Ernst, O. P. & Hubbell, W. L. Sequence of late molecular events in the activation of rhodopsin. *Proc. Natl. Acad. Sci.* **104**, 20290–20295 (2007).
 23. Lohse, M. J. & Hofmann, K. P. Spatial and Temporal Aspects of Signaling by G-Protein-Coupled Receptors. *Mol. Pharmacol.* **88**, 572–578 (2015).
 24. Lohse, M. J., Maiellaro, I. & Calebiro, D. Kinetics and mechanism of G protein-coupled receptor activation. *Curr. Opin. Cell Biol.* **27**, 87–93 (2014).
 25. Bünemann, M., Bücheler, M. M., Philipp, M., Lohse, M. J. & Hein, L. Activation and Deactivation Kinetics of α 2A- and α 2C-Adrenergic Receptor-activated G Protein-activated Inwardly Rectifying K⁺ Channel Currents. *J. Biol. Chem.* **276**, 47512–47517 (2001).
 26. Yao, X. *et al.* Coupling ligand structure to specific conformational switches in the β 2-adrenoceptor. *Nat. Chem. Biol.* **2**, 417–422 (2006).
 27. Damian, M., Mary, S., Martin, A., Pin, J. P. & Banères, J. L. G protein activation by the leukotriene B4 receptor dimer: Evidence for an absence of trans-activation. *J. Biol. Chem.* **283**, 21084–21092 (2008).
 28. Bockenhauer, S., Fürstenberg, A., Yao, X. J., Kobilka, B. K. & Moerner, W. E. Conformational Dynamics of Single G Protein-Coupled Receptor in Solution. *J. Phys.*

- Chem. B* **115**, 13328–13338 (2011).
29. Nygaard, R. *et al.* The dynamic process of β 2-adrenergic receptor activation. *Cell* **152**, 532–542 (2013).
 30. Olofsson, L. *et al.* Fine tuning of sub-millisecond conformational dynamics controls metabotropic glutamate receptors agonist efficacy. *Nat. Commun.* **5**, 1–12 (2014).
 31. Vafabakhsh, R., Levitz, J. & Isacoff, E. Y. Conformational dynamics of a class C G-protein-coupled receptor. *Nature* **524**, 497–501 (2015).
 32. Manglik, A. *et al.* Structural insights into the dynamic process of β 2-adrenergic receptor signaling. *Cell* **161**, 1101–1111 (2015).
 33. Gregorio, G. G. *et al.* Single-molecule analysis of ligand efficacy in β 2AR-G-protein activation. *Nature* **547**, 68–73 (2017).
 34. Vilardaga, J. P., Bünemann, M., Krasell, C., Castro, M. & Lohse, M. J. Measurement of the millisecond activation switch of G protein-coupled receptors in living cells. *Nat. Biotechnol.* **21**, 807–812 (2003).
 35. Lohse, M. J., Nuber, S. & Hoffmann, C. Fluorescence / Bioluminescence Resonance Energy Transfer Techniques to Study G-Protein-Coupled Receptor Activation and Signaling. *Pharmacol. Rev.* **64**, 299–336 (2012).
 36. Lohse, M. J. *et al.* Kinetics of G-protein-coupled receptor signals in intact cells. *Br. J. Pharmacol.* **153**, 125–132 (2008).
 37. Pin, J. P. & Bettler, B. Organization and functions of mGlu and GABA B receptor complexes. *Nature* **540**, 60–68 (2016).

38. Tateyama, M., Abe, H., Nakata, H., Saito, O. & Kubo, Y. Ligand-induced rearrangement of the dimeric metabotropic glutamate receptor 1 α . *Nat. Struct. Mol. Biol.* **11**, 637–642 (2004).
39. Hlavackova, V. *et al.* Sequential inter- and intrasubunit rearrangements during activation of dimeric metabotropic glutamate receptor 1. *Sci. Signal.* **5**, 1–12 (2012).
40. Marcaggi, P., Mutoh, H., Dimitrov, D., Beato, M. & Knopfel, T. Optical measurement of mGluR1 conformational changes reveals fast activation, slow deactivation, and sensitization. *Proc. Natl. Acad. Sci.* **106**, 11388–11393 (2009).
41. Koehl, A. *et al.* Structural insights into the activation of metabotropic glutamate receptors. *Nature* (2019). doi:10.1038/s41586-019-0881-4
42. Christopoulos, A. *et al.* International union of basic and clinical pharmacology. XC. Multisite pharmacology: Recommendations for the nomenclature of receptor allosterism and allosteric ligands. *Pharmacol. Rev.* **66**, 918–947 (2014).
43. Tsien, R. Y. the Green Fluorescent Protein. *Annu. Rev. Biochem.* **67**, 509–544 (1998).
44. Shaner, N. C., Steinbach, P. A. & Tsien, R. Y. A guide to choosing fluorescent proteins. *Nat. Methods* **2**, 905–909 (2005).
45. Bajar, B. T. *et al.* Improving brightness and photostability of green and red fluorescent proteins for live cell imaging and FRET reporting. *Sci. Rep.* **6**, 1–12 (2016).
46. Shaner, N. C. *et al.* Improving the photostability of bright monomeric orange and red fluorescent proteins. *Nat. Methods* **5**, 545–551 (2008).
47. Gurskaya, N. G., Savitsky, A. P., Yanushevich, Y. G., Lukyanov, S. A. & Lukyanov, K. A. Color transitions in coral's fluorescent proteins by site-directed mutagenesis. *BMC*

- Biochem.* **2**, 1–7 (2001).
48. McKinney, S. A., Murphy, C. S., Hazelwood, K. L., Davidson, M. W. & Looger, L. L. A bright and photostable photoconvertible fluorescent protein. *Nat. Methods* **6**, 131–133 (2009).
 49. Shcherbakova, D. M., Shemetov, A. A., Kaberniuk, A. A. & Verkhusha, V. V. *Natural Photoreceptors as a Source of Fluorescent Proteins, Biosensors, and Optogenetic Tools. Annual Review of Biochemistry* **84**, (2015).
 50. Shinoda, H., Shannon, M. & Nagai, T. Fluorescent proteins for investigating biological events in acidic environments. *Int. J. Mol. Sci.* **19**, (2018).
 51. Shen, Y., Rosendale, M., Campbell, R. E. & Perrais, D. pHuji, a pH-sensitive red fluorescent protein for imaging of exo- and endocytosis. *J. Cell Biol.* **207**, 419–432 (2014).
 52. Burgstaller, S. *et al.* PH-Lemon, a Fluorescent Protein-Based pH Reporter for Acidic Compartments. *ACS Sensors* **4**, 883–891 (2019).
 53. Yu, X. *et al.* An engineered palette of metal ion quenchable fluorescent proteins. *PLoS One* **9**, 1–11 (2014).
 54. Ravikumar, Y. *et al.* FMN-Based fluorescent proteins as heavy metal sensors against mercury ions. *J. Microbiol. Biotechnol.* **26**, 530–539 (2015).
 55. Arosio, D. *et al.* Spectroscopic and structural study of proton and halide ion cooperative binding to GFP. *Biophys. J.* **93**, 232–244 (2007).
 56. Suzuki, T. *et al.* Development of cysteine-free fluorescent proteins for the oxidative environment. *PLoS One* **7**, (2012).

57. Cannon, M. B. Re-engineering redox-sensitive green fluorescent protein for improved response rate. *Protein Sci.* **15**, 45–57 (2006).
58. Reuter, W. H. *et al.* Utilizing redox-sensitive GFP fusions to detect in vivo redox changes in a genetically engineered prokaryote. *Redox Biol.* **26**, 0–9 (2019).
59. Ren, W. & Ai, H. W. Genetically encoded fluorescent redox probes. *Sensors (Switzerland)* **13**, 15422–15433 (2013).
60. Förster, T. Zwischenmolekulare Energiewanderung und Konzentrationsdepolarisation der Fluoreszenz. *Ann. Phys.* **463**, 116–119 (1961).
61. Stryer, L. Fluorescence Energy Transfer as a Spectroscopic Ruler. *Annu. Rev. Biochem.* **47**, 819–846 (1978).
62. Periasamy, A. Fluorescence resonance energy transfer microscopy: a mini review. *J. Biomed. Opt.* **6**, 287 (2001).
63. Pflieger, K. D. G. & Eidne, K. A. Illuminating insights into protein-protein interactions using bioluminescence resonance energy transfer (BRET). *Nat. Methods* **3**, 165–174 (2006).
64. Chen, T. W. *et al.* Ultrasensitive fluorescent proteins for imaging neuronal activity. *Nature* **499**, 295–300 (2013).
65. Marvin, J. S. *et al.* An optimized fluorescent probe for visualizing glutamate neurotransmission. (2013). doi:10.1038/NMETH.2333
66. Jing, M. *et al.* A genetically encoded fluorescent acetylcholine indicator for in vitro and in vivo studies. (2019). doi:10.1038/nbt.4184
67. Patriarchi, T. *et al.* Ultrafast neuronal imaging of dopamine dynamics with designed

- genetically encoded sensors. *Science* (80-.). **360**, (2018).
68. Canepari, M., Nelson, L., Papageorgiou, G., Corrie, J. E. T. & Ogden, D. Photochemical and pharmacological evaluation of 7-nitroindolinyland 4-methoxy-7-nitroindolinyl-amino acids as novel, fast caged neurotransmitters. *J. Neurosci. Methods* **112**, 29–42 (2001).
 69. Börner, S. *et al.* FRET measurements of intracellular cAMP concentrations and cAMP analog permeability in intact cells. *Nat. Protoc.* **6**, 427–438 (2011).
 70. Trigo, F. F., Corrie, J. E. T. & Ogden, D. Laser photolysis of caged compounds at 405 nm: Photochemical advantages, localisation, phototoxicity and methods for calibration. *J. Neurosci. Methods* **180**, 9–21 (2009).
 71. Rondard, P. *et al.* Coupling of agonist binding to effector domain activation in metabotropic glutamate-like receptors. *J. Biol. Chem.* **281**, 24653–24661 (2006).
 72. Fujinaga, M. *et al.* Synthesis and Evaluation of Novel Radioligands for Positron Emission Tomography Imaging of Metabotropic Glutamate Receptor Subtype 1 (mGluR1) in Rodent Brain. **1**, (2012).
 73. Kunishima, N. *et al.* Structural basis of glutamate recognition by a dimeric metabotropic glutamate receptor. *Nature* **407**, 971–977 (2000).
 74. Grushevskiy, E. O. *et al.* Stepwise activation of a class C GPCR begins with millisecond dimer rearrangement. *Proc. Natl. Acad. Sci. U. S. A.* **116**, 10150–10155 (2019).
 75. Ye, L., Van Eps, N., Zimmer, M., Ernst, O. P. & Scott Prosser, R. Activation of the A_{2A} adenosine G-protein-coupled receptor by conformational selection. *Nature* **533**, 265–268 (2016).

76. Staus, D. P. *et al.* Allosteric nanobodies reveal the dynamic range and diverse mechanisms of G-protein-coupled receptor activation. *Nature* **535**, 448–452 (2016).
77. Gómez-Santacana, X. *et al.* Illuminating Phenylazopyridines to Photoswitch Metabotropic Glutamate Receptors: From the Flask to the Animals. *ACS Cent. Sci.* **3**, 81–91 (2017).
78. Sungkaworn, T. *et al.* Single-molecule imaging reveals receptor-G protein interactions at cell surface hot spots. *Nature* **550**, 543–547 (2017).

CURRICULUM VITAE

Name Yevgenii Grushevskiy

Date of birth 29.04.1992

Place of birth Korsun-Shevchenkivskiy, Ukraine

Nationality Ukrainian

Current address Pistoriusstr. 110A, 13086 Berlin

E-mail address e.o.grushevsky@gmail.com

Current position PhD student (2015- present)

Location Institute of Pharmacology and Toxicology, University of Würzburg,
Würzburg, Germany

Title of PhD thesis Activation kinetics of G-protein-coupled receptors

Supervisors Martin J. Lohse
Katrin G. Heinze
Markus Sauer

Academic background BSc and MSc in Applied Mathematics and Physics, MIPT, Russia

Internship Intern at Photochemistry Center, Moscow, Russia

Working experience Research assistant, Bogomoletz Institute of Physiology, Kyiv,
Ukraine

Languages

Ukrainian (native)

Russian (fluent)

English (fluent)

German (basic)

Publications

- Möller J, Isbilir A, Sungkaworn T, Osberg B, Karathanasis C, Sunkara V, **Grushevskiy EO**, Bock A, Annibale A, Heilemann M, Schütte C, Lohse MJ. Single molecule μ -opioid receptor membrane-dynamics reveal agonist-specific dimer formation with superresolved precision. *Manuscript in submission*.
- **Grushevskiy EO**, Kukaj T, Schmauder R, Bock A, Zabel U, Schwabe T, Benndorf K, Lohse MJ (2019) Stepwise activation of a class C GPCR begins with millisecond dimer rearrangement. *Procl Natl Acad USA* 116 (20)10150-10155.
- Cherkas V, Grebenyuk S, Osypenko D, Dovgan AV, **Grushevskiy EO**, Yedutenko M, *et al.* (2018) Measurement of intracellular concentration of fluorescently-labeled targets in living cells. *PLoS ONE* 13(4): e0194031.
- **E. Grushevsky**, A. Dovgan, V. Cherkas, P. Belan. (2015) Dependence of hippocalcin signaling on the lipid composition of the plasma membrane. *Acta Physiol* 215, Issue Supplement S705, 5 / *Conference proceedings*

Awards

- German-Ukrainian Academic Society, Travel Grant and PhD contest 3d prize, Tübingen, 2019

- MDC/FMP Technology Transfer Workshop, Audience Award
2nd place, Berlin, 2017
- Federation of European Physiological Societies, Travel Grant,
Kaunas, 2015
- Ukrainian Biophysical Society, Best Scientific Report Award
(oral presentation), Lutsk, 2015
- Ukrainian Physiological Society, Best Scientific Report Award
(poster), Lviv, 2015
- National Academy of Sciences of Ukraine, State Scholarship,
Kyiv, 2013-2015
- Ministry of Science and Education of Russia, State Scholarship,
Moscow, 2009-2010

Oral presentations

- Annual German-Ukrainian Academic Society, Tübingen,
Germany, 2019
- SFB/TR166 retreat, Jena, Germany, 2019
- IDK “Receptor Dynamics - Emerging Paradigms for Novel
Drugs” Symposium, Prague, Czechia, 2016
- SFB/TR166 retreat, Masserberg, Germany, 2016
- Federation of European Physiological Societies meeting, Kaunas,
Lithuania, 2015
- VI meeting of Ukrainian Biophysical Society, Lutsk-Svityaz,
Ukraine, 2015

Poster presentations

- II international symposium on photopharmacology,

Vic-Barcelona, Spain, 2018

- IDK “Receptor Dynamics - Emerging Paradigms for Novel Drugs” Symposium, Montpellier, France, 2017
- Gordon research conference on molecular pharmacology, Il Ciocco, Italy, 2017
- GLISTEN meeting, Erlangen, Germany 2016
- German Pharm-Tox Summit, Berlin, 2016
- IDK “Receptor Dynamics - Emerging Paradigms for Novel Drugs” Symposium, Rehovot, Israel, 2015

Workshops

- ❖ Workshop ‘R statistical analysis basic’, Berlin, Germany, 2017
- ❖ Certified mouse course from German State Office for Health and Social Affairs, Berlin, Germany, 2017
- ❖ Workshop 'Cardiac Receptors and Autoantibodies: Measuring Assays and Therapeutic Approaches', Rudolf Virchow Center, Würzburg, Germany, 2016
- ❖ 6th Spring School 'Biophysical methods of research', NASU Institute of Physiology, Kyiv, Ukraine, 2012

Date and Signature.....

ACKNOWLEDGEMENTS

Foremost, I would like to express the deepest appreciation to my supervisor, Prof. Martin Lohse, who gave me the opportunity to complete the doctoral studies in his outstanding laboratory and who has been a great mentor and a PhD advisor. His guidance helped me in all the time of research and writing of this thesis. I would also like to thank him for his patience, enthusiasm and great sense of humor during our scientific discussions.

I would also like to thank the rest of my thesis committee: Prof. Katrin Heinze and Prof. Markus Sauer for their encouragement, insightful comments, and hard questions during our meetings. During these four years, their scientific works were always for me an example to look up to.

My sincere gratitude also goes to the research group of Prof. Klaus Benndorf in the University Hospital Jena for all the scientific discussions and time we had together during our fruitful collaboration.

I thank my fellow labmates and staff in Würzburg and Berlin: Christine Salomon, whose help in organizational issues was invaluable, Ulrike Zabel and Monika Frank who cloned so many DNA constructs, Ruth Pareja, Jan Möller, Ali Işbilir, Hannes Schihada, Katarina Nemes, Selma Anton, for not only being helpful specialists in their fields, but also for being great friends to rely on.

Наприкінці я хочу подякувати своїм батькам та сім'ї за любов та підтримку, без якої ця робота не була би можливою, і за можливості й знання, котрі вони мені надали з народження. Дисертація присвячується моїй безмежно коханій нареченій Юлії.